Metastable states and T = 0 hysteresis in the random-field Ising model on random graphs

F. Detcheverry, M.L. Rosinberg[a], and G. Tarjus

Laboratoire de Physique Théorique des Liquides, Université Pierre et Marie Curie, 4 place Jussieu, 75252 Paris Cedex 05, France

Abstract. We study the ferromagnetic random-field Ising model on random graphs of fixed connectivity z (Bethe lattice) in the presence of an external magnetic field H. We compute the number of single-spin-flip stable configurations with a given magnetization m and study the connection between the distribution of these metastable states in the $H - m$ plane (focusing on the region where the number is exponentially large) and the shape of the saturation hysteresis loop obtained by cycling the field between $-\infty$ and $+\infty$ at $T = 0$. The annealed complexity $\Sigma_A(m, H)$ is calculated for $z = 2, 3, 4$ and the quenched complexity $\Sigma_Q(m, H)$ for $z = 2$. We prove explicitly for $z = 2$ that the contour $\Sigma_Q(m, H) = 0$ coincides with the saturation loop. On the other hand, we show that $\Sigma_A(m, H)$ is irrelevant for describing, even qualitatively, the observable hysteresis properties of the system.

PACS. 75.10.Nr Spin-glass and other random models – 75.60.Ej Magnetization curves, hysteresis, Barkhausen and related effects – 05.50.+q Lattice theory and statistics (Ising, Potts, etc.)

1 Introduction

The dynamical properties of random and frustrated systems are dominated at low temperature by the presence of a multitude of metastable states. This complex energy landscape is responsible for the strong hysteresis effects observed in a variety of physical systems (magnets, superconductors, fluids in porous media, ...) under the action of an external driving field. Much insight into such behavior has been gained recently through studying the zero-temperature random-field Ising model (RFIM) in an external magnetic field, which is a simple prototype of a disordered system far from equilibrium. The energy landscape of the model may be explored by changing the field adiabatically, which results in a series of discrete Barkhausen jumps (avalanches) in the magnetization, each jump corresponding to a sudden move to a new metastable configuration. A remarkable feature of the RFIM at $T = 0$ is the existence of a disorder-induced phase transition in the magnetization hysteresis loop obtained by cycling the field from one saturated state to the oppositely magnetized state and back. In three and higher dimensions, there is a transition between a continuous loop at strong disorder and a discontinuous loop with a macroscopic jump in the magnetization at low disorder [1]. The jump (corresponding to a macroscopic avalanche in the system) disappears at some critical value of the dis-

order where universal scaling behavior is observed. This nonequilibrium phase transition has been studied in detail by renormalization group and by numerical simulations on hypercubic lattices [2]. Exact analytical calculations have also been performed in one dimension [3] and generalized to a Bethe lattice [4]: in this case, the transition only exists for $z \geq 4$, where z is the connectivity of the lattice. Such a transition has been observed in thin Co/CoO films [5] and Cu-Al-Mn alloys [6], and we have recently suggested [7] that it may also be associated to the change in the adsorption behavior of ^{4}He in dilute silica aerogels [8]. In all these systems, activated processes are too slow to allow thermal equilibration on experimental time scales, which makes the $T = 0$ RFIM a relevant model for understanding the out-of-equilibrium behavior.

There is an expected connection between the shape of the $T = 0$ hysteresis loop and the distribution of the metastable states in the field-magnetization plane [9]. This issue, however, has only attracted little attention so far [10,11]. For the RFIM with ferromagnetic interactions, the probability to find metastable states outside the hysteresis loop vanishes in the thermodynamic limit, as shown in Appendix A. But what is the situation *inside* the loop? Is the entropy density (associated with the number of metastable states) positive everywhere? The situation is especially intriguing in the low-disorder regime where a region around the origin becomes inaccessible to any field history that starts from the saturated states [12]. The aim

a e-mail: mlr@lptl.jussieu.fr

of this work is thus to calculate the number of metastable configurations with a fixed magnetization m per spin as a function of the external field H. We consider a Gaussian distribution of the random fields whose width R measures the "strength" of the disorder, and, in order to analyze the problem analytically (at least partially), we work on a Bethe lattice defined here as a random graph of fixed connectivity z [13], i.e. a random collection of N vertices, each vertex being connected to z other vertices. Such a graph has the structure of a branching tree locally and small loops are rare, with typical size of order $\log N$. Spin models on random graphs (both with fixed and fluctuating connectivity) have attracted much attention in recent years because they can be solved exactly though each spin interacts with a finite number of other spins like in real short-range, finite-dimensional systems. The metastable configurations of the Ising ferromagnet [14–16] and of spin glass models [16,17] have been studied in this framework, but, to the best of our knowledge, the ferromagnetic RFIM has not yet been considered (except for $z = 2$ and in zero external field [18]). Since there is no plaquette frustration in this case (contrary to spin glasses), loops should not play any significant role in the large-N limit and we expect the number of metastable states on a typical random graph with connectivity z to be the same as in the interior of a Cayley tree with branching ratio $z - 1$ [19].

As is usual with disordered systems, one has to distinguish between annealed and quenched averages, the disorder average being here over both the random-graph and the random-field distributions. The quenched average is the appropriate quantity describing the behavior of the typical disorder realizations. Specifically, we want to compute both the *average* number $\overline{\mathcal{N}(m, H)}$ and the *typical* number $e^{\overline{\ln \mathcal{N}(m, H)}}$ of single-spin-flip stable states with a given magnetization m. Since these numbers are expected to scale exponentially with the number N of spins (at least in some region of the $H - m$ plane), the basic quantities are the associated entropy densities, i.e. the annealed complexity $\Sigma_A(m, H) = \lim_{N \to \infty} 1/N \, \ln \overline{\mathcal{N}(m, H)}$ and the quenched complexity $\Sigma_Q(m, H) = \lim_{N \to \infty} 1/N \, \overline{\ln \mathcal{N}(m, H)}$. In the following, we present the results for the annealed complexity on random graphs with connectivity $z = 2, 3$ and 4. We shall see that the qualitative behavior changes for $z \geq 3$, although the recursion equations for the RFIM on a Bethe lattice predict that the macroscopic jump in the hysteresis loop only occurs for $z \geq 4$ [4]. This illustrates that the annealed quantity is unable to describe, even qualitatively, the typical behavior of the system: indeed, the probabilistic calculation of reference [4] describes the behavior of the magnetization which is a self-averaging quantity that converges to its typical value when $N \to \infty$. (Note that the crucial distinction between annealed and quenched averages was neglected in Ref. [11].) The analytical computation of the quenched complexity requires the introduction of replicas and is thus more complicated (alternatively, one could also use the cavity method as in Ref. [16]). For this reason, we carry out the complete calculation of $\Sigma_Q(m, H)$ for $z = 2$ only. We then show explicitly that the contour

$\Sigma_Q(m, H) = 0$ identifies with the saturation loop of the one-dimensional RFIM previously calculated by a probabilistic method [3]: the typical number of metastable states thus ceases to be exponential with the system size exactly on the saturation hysteresis loop. To our knowledge, this is the first time that such a result is proven exactly.

The rest of the paper is organized as follows. In Section 2 we introduce the model and describe the averaging procedure over the random graphs. In Section 3 we present the general formalism for computing the annealed and quenched complexities on such graphs. The analytical and numerical results for the one-dimensional chain ($z = 2$) are discussed in Section 4. In Section 5 we present the results for the annealed complexity for $z = 3$ and $z = 4$. We conclude in Section 6 by discussing the possible behavior of the quenched complexity for $z \geq 4$ in the low-disorder regime. The absence of metastable states outside the saturation hysteresis loop is proven in Appendix A. Appendices B and C are devoted to technical details of the quenched calculation for $z = 2$.

2 Model

We study the ferromagnetic RFIM described by the Hamiltonian

$$H = -J \sum_{i<j} n_{ij} s_i s_j - \sum_i (H + h_i) s_i, \qquad (1)$$

where $J > 0$, s_i $(i = 1, \ldots, N)$ are Ising spins placed on the vertices of a random graph, and the random fields h_i are drawn from the Gaussian probability distribution $P(h_i) = \exp(-h_i^2/2R^2)/\sqrt{2\pi}R$. The variable n_{ij} is equal to 1 if the sites i, j are connected and to 0 otherwise.

Following reference [17], the random graphs are built as follows. First, the elements n_{ij} of the connectivity matrix (with $n_{ij} = n_{ji}$, $i < j$) are chosen at random from the probability distribution $\mathcal{P}(n_{ij}) = (1 - \gamma/N)\delta(n_{ij}; 0) + (\gamma/N)\delta(n_{ij}; 1)$ where γ is some arbitrary number of order one and $\delta(p; q)$ is the Kronecker-δ: this defines an ensemble of graphs for which the local connectivity is a Poisson variable in the large-N limit, like in the Viana-Bray spin glass model [20]. One then selects the subset of graphs where the connectivity of each site is equal to z. The average value of a dynamical variable A is thus given by

$$\overline{A} = \frac{1}{\mathcal{M}(N, z, \gamma)} \left\langle \left\langle A \prod_{i=1}^N \delta \left(\sum_{j \neq i} n_{ij}; z \right) \right\rangle_\gamma \right\rangle_h, \qquad (2)$$

where $\langle . \rangle_\gamma$ and $\langle . \rangle_h$ denote the averages with respect to the distributions $\mathcal{P}(n_{ij})$ and $P(h_i)$, respectively. $\mathcal{M}(N, z, \gamma)$ is the average number of graphs with connectivity z that are generated for a given γ. This quantity was calculated in reference [17] in the large-N limit:

$$\lim_{N \to \infty} \frac{1}{N} \ln \mathcal{M}(N, z, \gamma) = \frac{z}{2}(\ln z + \ln \gamma - 1) - \ln z! - \frac{\gamma}{2}. \quad (3)$$

By construction, the value of $\overline{A}$ is independent of the choice of γ in the thermodynamic limit $N \to \infty$. In the following, we drop the explicit dependence on z and γ.

3 Formalism

In this section we present the general formalism for computing the number of metastable states of the Gaussian RFIM on random graphs. Since the quenched calculation is achieved by introducing replicas and using the identity $\ln x = \lim_{n \to 0}(x^n - 1)/n$, we compute directly the average $\overline{\mathcal{N}(m,H)^n}$ for a general integer n, and then treat separately the annealed ($n = 1$) and quenched ($n \to 0$) cases. Our method is inspired from reference [15] where a global order-parameter function is introduced that allows to address the quenched calculation.

3.1 Basic equations

A configuration is said to be metastable when its energy cannot be decreased by flipping a single spin, a definition consistent with the $T = 0$ Glauber dynamics used in the previous studies of the nonequilibrium RFIM [1–4]. Such a configuration is a local minimum of the energy surface where each spin i is aligned with its local field f_i defined by

$$f_i = J \sum_j n_{ij} s_j + h_i + H. \tag{4}$$

The nth moment of the number of metastable states averaged over disorder is thus given by

$$\overline{\mathcal{N}(H)^n} = \frac{\mathcal{D}_n(N,H)}{\mathcal{M}(N)} \tag{5}$$

with

$$\mathcal{D}_n(N,H) = \left\langle\!\!\left\langle \left[\sum_{s_i=\pm 1}\prod_{i=1}^{N}\Theta(f_i s_i)\right]^n \delta\left(\sum_{j\neq i}n_{ij};z\right)\right\rangle_\gamma\!\!\right\rangle_h$$
$$= \left\langle\!\!\left\langle \mathrm{Tr}\ \prod_{i,a}[\Theta(f_i^a s_i^a)]\,\delta\left(\sum_{j\neq i}n_{ij};z\right)\right\rangle_\gamma\!\!\right\rangle_h \tag{6}$$

where Tr stands for the summation over all possible values of the n-replicated spins s_i^a ($a = 1,...,n$), $f_i^a = J\sum_j n_{ij}s_j^a + h_i + H$, and $\Theta(x)$ is the Heaviside step function (i.e. $\Theta(x) = 1$ if $x > 0$ and 0 if $x < 0$). Since we consider a continuous distribution of the random fields, there is no need to specify the value $\Theta(0)$: the local field f_i is almost surely different from zero and the system has no marginally stable states whose energy does not change under any single-spin flip. We then use integral representations of the Dirac-δ and Kronecker-δ to rewrite

equation (6) as

$$\mathcal{D}_n(N,H) = \left\langle\!\!\left\langle \mathrm{Tr}\ \int\prod_{i,a}\left[dx_i^a\delta\,(x_i^a - f_i^a)\,\Theta\,(x_i^a s_i^a)\right]\right.\right.$$
$$\left.\left.\times\,\delta\left(\sum_{j\neq i}n_{ij};z\right)\right\rangle_\gamma\!\!\right\rangle_h$$
$$= \left\langle\!\!\left\langle \mathrm{Tr}\ \int\prod_{i,a}\left[dx_i^a dy_i^a\Theta\,(x_i^a s_i^a)\right]\right.\right.$$
$$\left.\left.\times\ e^{\sum_i \mathbf{y}_i\cdot(\mathbf{x}_i-\mathbf{f}_i)}\delta\left(\sum_{j\neq i}n_{ij};z\right)\right\rangle_\gamma\!\!\right\rangle_h$$
$$= \left\langle\!\!\left\langle \mathrm{Tr}\ \int\prod_{i,a}\left[dx_i^a dy_i^a d\lambda_i\Theta\,(x_i^a s_i^a)\right]\right.\right.$$
$$\left.\left.\times\,e^{\sum_i[\mathbf{y}_i\cdot(\mathbf{x}_i-\mathbf{f}_i)-\lambda_i(\sum_{j\neq i}n_{ij}-z)]}\right\rangle_\gamma\!\!\right\rangle_h \tag{7}$$

where the bold symbols denote vectors in replica space, e.g. $\mathbf{x}_i = (x_i^1, x_i^2,...,x_i^n)$. The integration ranges are $[-\infty, +\infty]$ for x_i^a, $[-i\infty, +i\infty]$ for y_i^a, $[0, 2i\pi]$ for λ_i, and for brevity the normalisation factors $1/(2i\pi)$ are absorbed in the infinitesimal elements dy_i^a and $d\lambda_i$. Inserting the definition of f_i^a (with $\mathbf{h}_i = h_i\mathbf{1}, \mathbf{H} = H\mathbf{1}$) and performing the average over the distribution $\mathcal{P}(n_{ij})$ yields

$$\mathcal{D}_n(N,H) = \left\langle \mathrm{Tr}\ \int\prod_{i,a}\left[dx_i^a dy_i^a d\lambda_i\Theta(x_i^a s_i^a)\right]\right.$$
$$\times\,e^{\sum_i[\lambda_i z + \mathbf{y}_i\cdot(\mathbf{x}_i - \mathbf{h}_i - \mathbf{H})]}$$
$$\left.\times\prod_{i<j}\left(1 - \frac{\gamma}{N} + \frac{\gamma}{N}e^{-\lambda_i-\lambda_j-J(\mathbf{y}_i.\mathbf{s}_j+\mathbf{y}_j.\mathbf{s}_i)}\right)\right\rangle_h$$
$$= \left\langle \mathrm{Tr}\int\prod_{i,a}\left[dx_i^a dy_i^a d\lambda_i\Theta(x_i^a s_i^a)\right]\right.$$
$$\times\,e^{\sum_i[\lambda_i z + \mathbf{y}_i\cdot(\mathbf{x}_i - \mathbf{h}_i - \mathbf{H})]}$$
$$\left.\times \exp\left(-\frac{\gamma N}{2} + \frac{\gamma}{2N}\sum_{i,j}e^{-\lambda_i-\lambda_j-J(\mathbf{y}_i.\mathbf{s}_j+\mathbf{y}_j.\mathbf{s}_i)}\right)\right\rangle_h \tag{8}$$

where terms that are negligible in the thermodynamic limit have been dropped in the last exponential.

Like in reference [15] we now introduce an "order-parameter" function $c(\boldsymbol{\sigma},\boldsymbol{\tau}) = (1/N)\sum_i\delta(\boldsymbol{s}_i;\boldsymbol{\sigma})\exp[-(\lambda_i + J\mathbf{y}_i.\boldsymbol{\tau})]$, where $\boldsymbol{\sigma}$ and $\boldsymbol{\tau}$ are binary vectors in replica space (i.e. $\sigma^a, \tau^a = \pm 1$). Then,

$$\exp\left[-\frac{\gamma N}{2} + \frac{\gamma}{2N}\sum_{i,j}e^{-\lambda_i-\lambda_j-J(\mathbf{y}_i.\mathbf{s}_j+\mathbf{y}_j.\mathbf{s}_i)}\right] =$$
$$\exp\left[-\frac{\gamma N}{2} + \frac{\gamma N}{2}\sum_{\boldsymbol{\sigma},\boldsymbol{\tau}}c(\boldsymbol{\sigma},\boldsymbol{\tau})c(\boldsymbol{\tau},\boldsymbol{\sigma})\right], \tag{9}$$

a relation that we use to decouple the sum over the site labels i and j and perform the trace over a single spin only in each replica. As outlined in the Appendix of reference [15], the $2n$-variable function $c(\boldsymbol{\sigma}, \boldsymbol{\tau})$ may be inserted in equation (8) via integrals over δ-functions represented by Fourier integrals over other auxiliary functions. After some formal manipulations, we obtain

$$
\mathcal{D}_n(N, H) =
$$

$$
\int \prod_{\boldsymbol{\sigma}, \boldsymbol{\tau}} \left[dc(\boldsymbol{\sigma}, \boldsymbol{\tau}) \right] \exp \left\{ -\frac{\gamma N}{2} \sum_{\boldsymbol{\sigma}, \boldsymbol{\tau}} c(\boldsymbol{\sigma}, \boldsymbol{\tau}) c(\boldsymbol{\tau}, \boldsymbol{\sigma}) - \frac{\gamma N}{2} \right\}
$$

$$
\times \left[\sum_{\boldsymbol{\sigma}} \int P(h) dh \int d\mathbf{x} d\mathbf{y} d\lambda \exp \left\{ \lambda z + \mathbf{y}.(\mathbf{x} - \mathbf{h} - \mathbf{H}) \right.\right.
$$

$$
\left.\left. + \gamma e^{-\lambda} \sum_{\boldsymbol{\tau}} c(\boldsymbol{\tau}, \boldsymbol{\sigma}) e^{-J\mathbf{y}.\boldsymbol{\tau}} \right\} \prod_a \Theta(x^a \sigma^a) \right]^N \quad (10)
$$

which may be computed in the thermodynamic limit as a saddle-point integral. This leads to

$$
\lim_{N \to \infty} \frac{1}{N} \ln \mathcal{D}_n(N, H) =
$$

$$
\max_{c(\boldsymbol{\sigma}, \boldsymbol{\tau})} \left\{ -\frac{\gamma}{2} \sum_{\boldsymbol{\sigma}, \boldsymbol{\tau}} c(\boldsymbol{\sigma}, \boldsymbol{\tau}) c(\boldsymbol{\tau}, \boldsymbol{\sigma}) - \frac{\gamma}{2} + \Lambda[c] \right\}, \quad (11)
$$

with

$$
\Lambda[c] = \ln \sum_{\boldsymbol{\sigma}} \int P(h) dh \int d\mathbf{x} d\mathbf{y} d\lambda \exp\{\lambda z + \mathbf{y}.(\mathbf{x} - \mathbf{h} - \mathbf{H})
$$

$$
+ \gamma e^{-\lambda} \sum_{\boldsymbol{\tau}} c(\boldsymbol{\tau}, \boldsymbol{\sigma}) e^{-J\mathbf{y}.\boldsymbol{\tau}} \} \prod_a \Theta(x^a \sigma^a). \quad (12)
$$

Using the identity [14]

$$
\frac{1}{2i\pi} \int_0^{2i\pi} d\lambda e^{\lambda z + \alpha e^{-\lambda}} = \frac{\alpha^z}{z!}, \quad (13)
$$

we get

$$
\Lambda[c] = \ln \frac{\gamma^z}{z!} + \ln \sum_{\boldsymbol{\sigma}} \int P(h) dh \int d\mathbf{x} d\mathbf{y} \; e^{\mathbf{y}.(\mathbf{x} - \mathbf{H} - \mathbf{h})}
$$

$$
\times \sum_{\boldsymbol{\tau}_1 ... \boldsymbol{\tau}_z} c(\boldsymbol{\tau}_1, \boldsymbol{\sigma}) ... c(\boldsymbol{\tau}_z, \boldsymbol{\sigma}) e^{-J\mathbf{y}.[\boldsymbol{\tau}_1 + \boldsymbol{\tau}_2 + ... \boldsymbol{\tau}_z]} \prod_a \Theta(x^a \sigma^a),
$$

$$
(14)
$$

and the integrations over $\mathbf{y}$ (giving δ functions again) and then over $\mathbf{x}$ may be performed to finally obtain

$$
\Lambda[c] = \ln \frac{\gamma^z}{z!} + \ln \sum_{\boldsymbol{\sigma}, \boldsymbol{\tau}_1 ... \boldsymbol{\tau}_z} c(\boldsymbol{\tau}_1, \boldsymbol{\sigma}) ... c(\boldsymbol{\tau}_z, \boldsymbol{\sigma})
$$

$$
\times \int P(h) dh \prod_a \Theta \left[\left(H + h + J \sum_{l=1}^z \tau_l^a \right) \sigma^a \right]. \quad (15)
$$

Note that the random field distribution $P(h)$ has not yet been specified at this stage.

It is straightforward to generalize the preceding calculation for a fixed magnetization m. $\mathcal{D}_n(N, m, H)$ is now defined as

$$
\mathcal{D}_n(N, m, H) = \left\langle \left\langle \left[\sum_{s_i = \pm 1} \prod_{i=1}^N \Theta \left(f_i s_i \right) \right.\right.\right.
$$

$$
\left.\left.\left. \times \delta \left(\sum_i s_i - Nm \right) \right]^n \delta \left(\sum_{j \neq i} n_{ij} - z \right) \right\rangle_{\gamma'} \right\rangle_h \quad (16)
$$

and the δ-function constraint on $\sum_i s_i$ may be relaxed by introducing a Lagrange multiplier g coupled to the magnetization (see, e.g, Ref. [14]). The whole calculation is quite similar to the one presented above and equation (11) becomes

$$
\lim_{N \to \infty} \frac{1}{N} \ln \mathcal{D}_n(N, m, H) =
$$

$$
\max_{c(\boldsymbol{\sigma}, \boldsymbol{\tau}), \mathbf{g}} \left\{ -\frac{\gamma}{2} \sum_{\boldsymbol{\sigma}, \boldsymbol{\tau}} c(\boldsymbol{\sigma}, \boldsymbol{\tau}) c(\boldsymbol{\tau}, \boldsymbol{\sigma}) \right.
$$

$$
\left. -\frac{\gamma}{2} - m \sum_a g^a + \Lambda[c, \mathbf{g}] \right\}, \quad (17)
$$

with

$$
\Lambda[c, \mathbf{g}] = \ln \frac{\gamma^z}{z!} + \ln \sum_{\boldsymbol{\sigma}, \boldsymbol{\tau}_1 ... \boldsymbol{\tau}_z} c(\boldsymbol{\tau}_1, \boldsymbol{\sigma}) ... c(\boldsymbol{\tau}_z, \boldsymbol{\sigma})
$$

$$
\times \int P(h) dh \prod_a e^{g^a \sigma^a} \Theta \left[\left(H + h + J \sum_{l=1}^z \tau_l^a \right) \sigma^a \right] \quad (18)
$$

where $\mathbf{g} = (g^1, g^2, ..., g^n)$. As can be seen immediately, equations (11) and (15) are recovered when $\mathbf{g} = \mathbf{0}$ and thus equations (17-18) may be used as the starting point of further analysis.

Extremization with respect to $c(\boldsymbol{\sigma}, \boldsymbol{\tau})$ readily gives

$$
c(\boldsymbol{\sigma}, \boldsymbol{\tau}) = e^{-\Lambda} \frac{\gamma^{z-1}}{(z-1)!}
$$

$$
\times \sum_{\boldsymbol{\tau}_1 ... \boldsymbol{\tau}_{z-1}} c(\boldsymbol{\tau}_1, \boldsymbol{\sigma}) ... c(\boldsymbol{\tau}_{z-1}, \boldsymbol{\sigma}) F_z(\boldsymbol{\sigma}, \boldsymbol{\tau}, \boldsymbol{\tau}_1 ... \boldsymbol{\tau}_{z-1}) \quad (19)
$$

with

$$
F_z(\boldsymbol{\sigma}, \boldsymbol{\tau}, \boldsymbol{\tau}_1 ... \boldsymbol{\tau}_{z-1}) =
$$

$$
\int P(h) dh \prod_a e^{g^a \sigma^a} \Theta \left[\left(H + h + J \left(\tau^a + \sum_{l=1}^{z-1} \tau_l^a \right) \right) \sigma^a \right],
$$

$$
(20)
$$

which in turn yields the normalization condition

$$
\frac{\gamma}{z} \sum_{\boldsymbol{\sigma}, \boldsymbol{\tau}} c(\boldsymbol{\sigma}, \boldsymbol{\tau}) c(\boldsymbol{\tau}, \boldsymbol{\sigma}) = 1. \quad (21)
$$

Likewise, extremization with respect to g^a yields

$$m = \partial \Lambda[c, \mathbf{g}] / \partial g^a$$

$$= e^{-\Lambda} \frac{\gamma^z}{z!} \sum_{\boldsymbol{\sigma}, \boldsymbol{\tau}_1 \dots \boldsymbol{\tau}_z} \sigma^a c(\boldsymbol{\tau}_1, \boldsymbol{\sigma}) \dots c(\boldsymbol{\tau}_z, \boldsymbol{\sigma})$$

$$\times \int P(h) dh \prod_a e^{g^a \sigma^a} \Theta \left[\left(H + h + J \sum_{l=1}^{z} \tau_l^a \right) \sigma^a \right]$$

$$= \sum_{\boldsymbol{\sigma}, \boldsymbol{\tau}} \sigma^a c(\boldsymbol{\sigma}, \boldsymbol{\tau}) c(\boldsymbol{\tau}, \boldsymbol{\sigma}) / \sum_{\boldsymbol{\sigma}, \boldsymbol{\tau}} c(\boldsymbol{\sigma}, \boldsymbol{\tau}) c(\boldsymbol{\tau}, \boldsymbol{\sigma}) \qquad (22)$$

with $a = 1, \dots, n$.

Inserting equation (21) into equation (17) and using equations (3) and (5), we finally obtain in the large-N limit

$$\overline{\mathcal{N}(m, H)^n} \sim \exp \left[N \max_{c(\boldsymbol{\sigma}, \boldsymbol{\tau}), \boldsymbol{g}} \left\{ \Lambda[c, \boldsymbol{g}] - m \sum_a g^a \right. \right.$$
$$\left. \left. - \frac{z}{2} (\ln z + \ln \gamma) + \ln z! \right\} \right]. \qquad (23)$$

3.2 Annealed complexity

We first consider the case $n = 1$ corresponding to the annealed average. $\boldsymbol{\sigma}$ and $\boldsymbol{\tau}$ become standard Ising variables σ, τ and the preceding equations simplify considerably. In particular, the function $c(\sigma, \tau)$ can only take four distinct values which we denote c_{++}, c_{+-}, c_{-+}, and c_{--}. Performing the integration over the random field distribution, equation (18) becomes

$$\Lambda[c, g] = \ln \frac{\gamma^z}{z!} + \ln \sum_{\sigma, \tau_1 \dots \tau_z = \pm 1} e^{g\sigma} c(\tau_1, \sigma) \dots c(\tau_z, \sigma)$$

$$\times \frac{1}{2} \left[1 + \mathrm{erf} \left(\frac{[H + J \sum_1^z \tau_k] \sigma}{R \sqrt{2}} \right) \right]$$

$$= \ln \frac{\gamma^z}{z!} + \ln \left[e^g c_{-+}^z f_+ \left(\frac{c_{++}}{c_{-+}} \right) \right.$$

$$\left. + e^{-g} c_{+-}^z f_- \left(\frac{c_{--}}{c_{+-}} \right) \right] \qquad (24)$$

where $\mathrm{erf}(x) = (2/\sqrt{\pi}) \int_0^x e^{-t^2} dt$ is the error function and the functions $f_{\pm}(x)$ are defined by

$$f_{\pm}(x) = \frac{1}{2} \sum_{n=0}^{z} \binom{z}{n} x^n \left[1 + \mathrm{erf} \left(\frac{J(2n - z) \pm H}{R \sqrt{2}} \right) \right]. \qquad (25)$$

Like in reference [14] we now change to the new variables $u = c_{++}/c_{-+}$, $v = c_{--}/c_{+-}$, $t = c_{+-}/c_{-+}$, solve the saddle point equation for c_{-+}, and substitute the result in equation (23). We then find that the dependence on γ disappears (as it must be), and the average number of

metastable states with magnetization m is given in the large-N limit by $\overline{\mathcal{N}(m, H)} \sim \exp[\Sigma_A(m, H) N]$ with

$$\Sigma_A(m, H) = \max_{u, v, t, g} \left\{ -\frac{z}{2} \ln \left(u^2 + t^2 v^2 + 2t \right) \right.$$
$$\left. + \ln[f_+(u) e^g + t^z f_-(v) e^{-g}] - gm \right\}. \qquad (26)$$

Solving the stationarity condition with respect to g gives

$$g = \frac{1}{2} \left[z \ln t + \ln \frac{1+m}{1-m} - \ln \frac{f_+(u)}{f_-(v)} \right], \qquad (27)$$

and substituting into equation (26) we finally obtain

$$\Sigma_A(m, H) = \max_{u, v, t} \left\{ -\frac{z}{2} \ln \left(u^2 + t^2 v^2 + 2t \right) \right.$$
$$+ \frac{1+m}{2} \ln f_+(u) + \frac{1-m}{2} \ln f_-(v)$$
$$\left. + z \frac{1-m}{2} \ln t - \frac{1+m}{2} \ln \frac{1+m}{2} - \frac{1-m}{2} \ln \frac{1-m}{2} \right\}. \qquad (28)$$

The saddle point equations $\partial \Sigma_A / \partial v = 0$ and $\partial \Sigma_A / \partial t = 0$ may be solved analytically to give $t = t(v) = f'_-(v)/[zv f_-(v) - v^2 f'_-(v)]$ and $u = [(1 + m)t^2 v^2 + 2mt]^{1/2}/[1-m]^{1/2}$ (the negative branch of u leads to solutions that have no physical meaning). On the other hand, the remaining equation, $\partial \Sigma_A / \partial u = 0$, must be solved numerically.

The total complexity $\Sigma_A^{max}(H)$ also corresponds to the maximum of $\Sigma_A(m, H)$. It is given by equation (26) with $g = 0$; one can associate to this maximum a value of the magnetization $m_A(H)$, which is then obtained by solving equation (27). One still has $t = t(v)$ but the saddle point equations for u and v must be solved numerically. For $H = 0$ however, these equations admit the solution $u = v$ and one has to solve the unique equation $t(v) = 1$. As in the case of the pure ferromagnet [14], this solution corresponds to the fixed point of the transformation $u \to v$, $v \to u$, $t \to 1/t$ which leaves $\Sigma_A^{max}(H = 0)$ invariant (when $R \neq 0$, this is the only solution of the saddle point equations).

3.3 Quenched complexity

We now turn to the calculation of the quenched complexity given by

$$\Sigma_Q(m, H) = \lim_{N \to \infty} \frac{1}{N} \lim_{n \to 0} \frac{1}{n} \left[\overline{\mathcal{N}(m, H)^n} - 1 \right] \qquad (29)$$

where, as usual, the order of the limits $N \to \infty$ and $n \to 0$ is inverted and the expression of $\overline{\mathcal{N}(m, H)^n}$ is extended to non-integer n to allow the limit $n \to 0$ to be taken. Some ansatz concerning the form of the solution of the saddle point equation (19) as $n \to 0$ is now required. As alluded to in the Introduction, a major difference between the ferromagnetic RFIM and spin-glass models comes from the

role of frustration. For the Bethe lattice spin-glass [13], frustration (due to the presence of large loops) induces a replica symmetry breaking instability similar to the one found in the fully-connected Sherrington-Kirkpatrick model and corresponding to the appearance of an exponential number of *pure* states. On the other hand, for the RFIM, this phenomenon does not occur in the infinite-range model [22], nor on finite-connectivity lattices at the mean-field level (it may be checked for instance that the number of pure states on the Bethe lattice is indeed non-exponential [23]). We thus assume that the solution of equation (19) remains invariant with respect to the permutation of the replica indices when $n \to 0$. Setting $g^a = g$ in equation (23), we then obtain

$$
\Sigma_Q(m, H) =
$$

$$
\max_g \left\{ -mg + \lim_{n \to 0} \frac{1}{n} \left[\Lambda^*(g) - \frac{z}{2}(\ln z + \ln \gamma) + \ln z! \right] \right\}
$$

$$
= \Lambda_1^*(g^*) - m g^* \tag{30}
$$

where $\Lambda^*(g) = \Lambda_0^* + n\Lambda_1^*(g) + O(n^2)$ is the value of Λ at the saddle-point solution $c^*(\boldsymbol{\sigma}, \boldsymbol{\tau})$ and g^* is the position of the maximum of $\Lambda^*(g)$. The second line of this equation also uses the relation $\Lambda_0^* = \frac{z}{2}(\ln z + \ln \gamma) - \ln z!$, which is a necessary condition for the $n \to 0$ limit to exist and be independent of γ. Note that equation (30) corresponds to a Legendre transformation between Σ_Q and Λ_1^*, so that the stationarity condition $\partial \Lambda_1^*/\partial g^* = m$ implies that $\partial \Sigma_Q(m, H)/\partial m = -g^*$. In fact, as will be illustrated below, it is convenient to consider that both Σ_Q and m are parameterized by g (to simplify the notations, the superscript * is dropped in the following), with g going from $-\infty$ to $+\infty$. One then has the overall symmetry $\Sigma_Q(-g, -H) = \Sigma_Q(g, H)$, $m(-g, -H) = m(g, H)$, and the maximum number of metastable states is obtained by setting $g = 0$.

The main consequence of replica-symmetry is that $c(\boldsymbol{\sigma}, \boldsymbol{\tau})$ is a function of the three variables $s = \sum_{a=1}^n \sigma^a$, $u = \sum_{a=1}^n \sigma^a \tau^a$, $t = \sum_{a=1}^n \tau^a$ only. This suggests, following reference [15], to introduce an integral representation of $c(s, u, t)$ so as to perform an analytic continuation of this function on the imaginary axis in the small n limit where s, u, and t may be treated as continuous variables. It turns out, however, that the situation is not that simple here because of the constraints on the values of σ^a and τ^a. To illustrate the problem, let us consider the case $z = 2$. Equation (19) then reads

$$
c(\boldsymbol{\sigma}, \boldsymbol{\tau}) = \gamma e^{-\Lambda} \sum_{\boldsymbol{\tau}_1} c(\boldsymbol{\tau}_1, \boldsymbol{\sigma}) F_2(\boldsymbol{\sigma}, \boldsymbol{\tau}, \boldsymbol{\tau}_1) \tag{31}
$$

with

$$
F_2(\boldsymbol{\sigma}, \boldsymbol{\tau}, \boldsymbol{\tau}_1) = e^{gs} \int P(h) dh \prod_a \Theta[(H + h + J(\tau + \tau_1^a))\sigma^a]. \tag{32}
$$

Performing the integration over the random field distribu-

tion in the four regions $h < -2J - H$, $-2J - H < h < -H$, $-H < h < 2J - H$, and $2J - H < h$, we obtain

$$
F_2(\boldsymbol{\sigma}, \boldsymbol{\tau}, \boldsymbol{\tau}_1) = \frac{1 - a}{2} e^{-gn}
$$

$$
\times \prod_a \delta(\sigma^a; -1) + \frac{1 - c}{2} e^{gn} \prod_a \delta(\sigma^a; 1)
$$

$$
+ \frac{a - b}{2} e^{gs} \prod_a \left[\delta(\sigma^a; -1)\delta(\tau_1^a; -\tau^a) + \delta(\tau_1^a; \tau^a)\delta(\tau^a; \sigma^a) \right]
$$

$$
+ \frac{b + c}{2} e^{gs} \prod_a \left[\delta(\sigma^a; 1)\delta(\tau_1^a; -\tau^a) + \delta(\tau_1^a; \tau^a)\delta(\tau^a; \sigma^a) \right] \tag{33}
$$

where $a = \mathrm{erf}((2J + H)/R\sqrt{2})$, $b = \mathrm{erf}(H/R\sqrt{2})$, and $c = \mathrm{erf}((2J - H)/R\sqrt{2})$. With this, equation (31) reads

$$
\frac{e^\Lambda}{\gamma} c(\boldsymbol{\sigma}, \boldsymbol{\tau}) = \frac{1 - a}{2} e^{-gn} \prod_a \delta(\sigma^a; -1) \sum_{\boldsymbol{\tau}_1} c(\boldsymbol{\tau}_1, -\mathbf{1})
$$

$$
+ \frac{1 - c}{2} e^{gn} \prod_a \delta(\sigma^a; 1) \sum_{\boldsymbol{\tau}_1} c(\boldsymbol{\tau}_1, \mathbf{1})
$$

$$
+ \frac{a - b}{2} e^{gs} \sum_{\boldsymbol{\tau}_1} c(\boldsymbol{\tau}_1, \boldsymbol{\sigma})
$$

$$
\times \prod_a \left[\delta(\sigma^a; -1)\delta(\tau_1^a; -\tau^a) + \delta(\tau_1^a; \tau^a)\delta(\tau^a; \sigma^a) \right]
$$

$$
+ \frac{b + c}{2} e^{gs} \sum_{\boldsymbol{\tau}_1} c(\boldsymbol{\tau}_1, \boldsymbol{\sigma})
$$

$$
\times \prod_a \left[\delta(\sigma^a; 1)\delta(\tau_1^a; -\tau^a) + \delta(\tau_1^a; \tau^a)\delta(\tau^a; \sigma^a) \right] \tag{34}
$$

where $\pm \mathbf{1} = (\pm 1, \dots \pm 1)$. The difficulty comes from the presence of the Kronecker-δ's that precludes any straightforward use of a Fourier representation of $c(\boldsymbol{\tau}, \boldsymbol{\sigma})$ in the limit $n \to 0$. Because of this, we have to work out the self-consistent equation (19) *before* taking the small n limit, a nontrivial (if not unsolvable) task for a generic value of the connectivity. In fact, only the case $z = 2$ seems to be simple enough to be handled analytically. Inspection of equation (34) suggests that the solution has the form

$$
\sqrt{\frac{\gamma}{2}} c(\boldsymbol{\sigma}, \boldsymbol{\tau}) =
$$

$$
A \prod_a \delta(\sigma^a; -1) + B e^{gs} \prod_a \delta(\sigma^a; \tau^a) + C \prod_a \delta(\sigma^a; 1)
$$

$$
+ D(\boldsymbol{\sigma}, \boldsymbol{\tau}) \prod_a \left[\delta(\sigma^a; -1)\delta(\tau^a; 1) + \delta(\tau^a; \sigma^a) \right]
$$

$$
+ E(\boldsymbol{\sigma}, \boldsymbol{\tau}) \prod_a \left[\delta(\sigma^a; 1)\delta(\tau^a; -1) + \delta(\tau^a; \sigma^a) \right], \tag{35}
$$

which in turn, together with equation (21), yields a set of six coupled equations for the unknown quantities $\Lambda, A, B, C, D(\boldsymbol{\sigma}, \boldsymbol{\tau}), E(\boldsymbol{\sigma}, \boldsymbol{\tau})$. It is only at this stage that the $n \to 0$ limit may be taken, noticing that $D(\boldsymbol{\sigma}, \boldsymbol{\tau})$ and $E(\boldsymbol{\sigma}, \boldsymbol{\tau})$ are functions of two variables only (say, s and t)

instead of three because of the constraints on $\boldsymbol{\sigma}$ and $\boldsymbol{\tau}$ that are imposed by the Kronecker-δ (it is easy to check that the third variable $u = n - |s - t|$). We then introduce the integral representations

$$D(s,t) = \int dxdy \hat{D}(x,y)e^{xs+yt} ,$$

$$E(s,t) = \int dxdy \hat{E}(x,y)e^{xs+yt} \quad (36)$$

where $\hat{D}(x,y)$ and $\hat{E}(x,y)$ are the Fourier transforms of $D(s,t)$ and $E(s,t)$ when $n \to 0$,

$$\hat{D}(x,y) = \int \frac{ds}{2\pi} \frac{dt}{2\pi} D(is,it)e^{-i(sx+ty)},$$

$$\hat{E}(x,y) = \int \frac{ds}{2\pi} \frac{dt}{2\pi} E(is,it)e^{-i(sx+ty)}, \quad (37)$$

and we expand all quantities at order n (i.e. $A = A_0 + nA_1 + O(n^2), ..., \hat{E}(x,y) = \hat{E}_0(x,y) + n\hat{E}_1(x,y) + O(n^2)$) as detailed in Appendix B. This allows one to solve the equations at the first two orders in n and, after some lengthy algebra, to compute $\Lambda_1(g)$ (see Eq. (B25)) from which we finally get

$$\Sigma_Q(g,H) = \frac{1}{2}\left[1 + b + \frac{(1-a)(b+c)}{a-b}\right]$$

$$\times \left[S_3(g) - g\frac{\partial S_3(g)}{\partial g}\right] \quad (38)$$

where $S_3(g) = \int dxdy \hat{D}_0(x,y)\ln[2\cosh x]$. A closed expression of $m(g,H)$ (Eq. B27) may be also obtained from equation (22), but it contains more complicated integrals of $\hat{D}_0(x,y)$ and it is in fact more convenient to compute the magnetization by numerically differentiating the expression (B25) of $\Lambda_1(g)$ with respect to g.

The only remaining task consists in solving numerically the coupled integral equations satisfied by $\hat{D}_0(x,y)$ and $\hat{E}_0(x,y)$. This is outlined in Appendix C.

4 Results for the one-dimensional chain ($z = 2$)

When $z = 2$ the Bethe lattice is just a collection of disconnected closed loops. In the thermodynamic limit, the dominant contributions to self-averaging quantities come from the loops of macroscopic size, and one thus expects the results to be the same as for the one-dimensional RFIM. Although no phase transitions occur in one dimension, frustration makes the problem nontrivial, and the relation between the shape of the hysteresis loop and the distribution of the metastable states can be fully elucidated. Note that the typical number of metastable states of the random-field Ising chain and their distribution in magnetization and energy were computed a few years ago by a numerical transfer-matrix method [18], but the study was
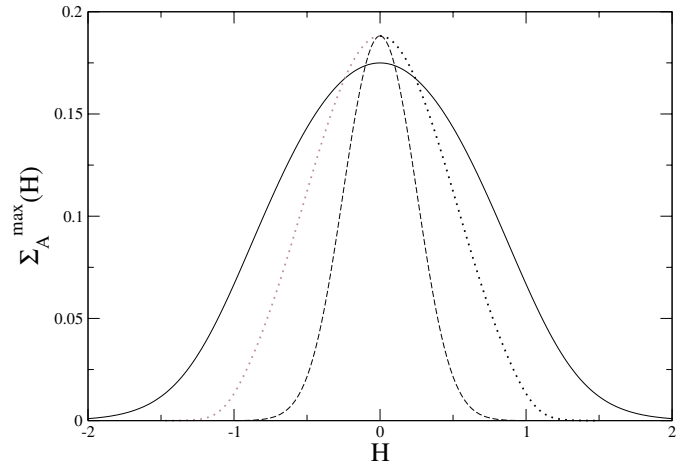

Fig. 1. Total annealed complexity $\Sigma_A^{max}(H)$ for $z = 2$ and $R = 1$ (solid line), 0.5 (dotted line) and 0.25 (dashed line).

restricted to the case of zero external field: therefore, the relation with the $T = 0$ hysteretic behavior was not investigated. Moreover, some results of reference [18] appear to violate the convexity inequality $\overline{\ln \mathcal{N}} \leq \ln \overline{\mathcal{N}}$, as will be shown in the following.

4.1 Annealed complexity

Let us first consider the total annealed complexity $\Sigma_A^{max}(H)$ as obtained from equation (26) with $g = 0$. Its dependence on H is illustrated in Figure 1 for different values of the disorder strength R (hereafter we take $J = 1$ in the numerical applications). It can be seen that the presence of the magnetic field reduces the total number of metastable states, in agreement with the expectation that a sufficiently large field imposes the existence of a unique state. As R decreases, the metastable states concentrate in the vicinity of $H = 0$ and in the limit $R \to 0$ they are completely destroyed by an infinitesimal field. From the solution of the equation $t(v) = 1$, the zero-field complexity is given by

$$\Sigma_A^{max}(H = 0) = \ln\left[\frac{1}{2} + \frac{1}{2}\sqrt{1 + \mathrm{erf}^2\left(\frac{J\sqrt{2}}{R}\right)}\right], \quad (39)$$

in agreement with a recent transfer matrix calculation [21]. It may be noted that this quantity approaches $\ln \frac{1+\sqrt{2}}{2} \approx 0.188$ when $R \to 0$, a value much smaller than the complexity of the pure ferromagnet, $\Sigma_{R=0}^{max}(H = 0) = \ln \frac{1+\sqrt{5}}{2} \approx 0.481$ [14,17]. This singular behavior of the zero-field complexity computed from equations (25–28) in the limit $R \to 0$ comes from the fact that marginal states, absent when $R \neq 0$, are not properly counted when $R = 0$: indeed, $f(x) = [1 + \mathrm{erf}(x/R\sqrt{2})]/2 \to \Theta(x)$ for $x \neq 0$ whereas $f(0) = 1/2$; to also include in our calculation the marginal states that exist in the pure system, one should instead set $\Theta(0) = 1$ as in reference [14]. Actually, all metastable states are marginal in the Ising chain at zero
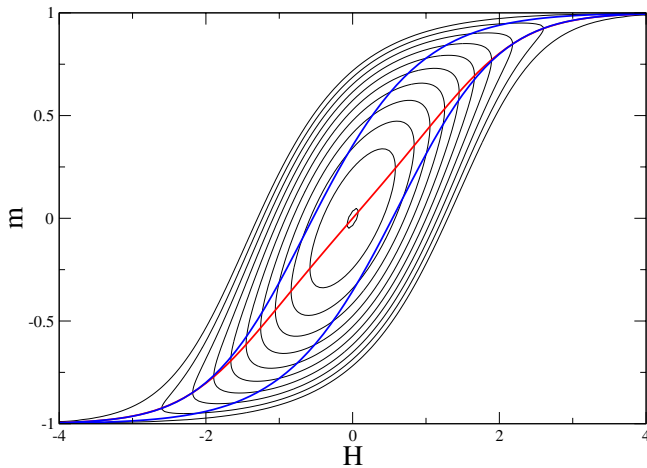
Fig. 2. (Color online) Projection of $\Sigma_A(m, H)$ onto the $H-m$ plane for $z = 2$ and $R = 2$. The contours are separated by 10^{-2} (with $\Sigma_A(0,0) \approx 0.100$). The red curve is the locus $m_A(H)$ of the maxima of $\Sigma_A(m, H)$. The blue curve is the $T = 0$ saturation hysteresis loop calculated in reference [3].

Fig. 3. Annealed (solid line) and quenched (dashed line) complexities in zero external field for $z = 2$ and $R = 2$ as a function of magnetization.

field (they simply correspond to different positions of the walls separating domains of up and down spins) and one can directly calculate a "biased" complexity by associating to each domain wall an arbitrary weight p with $0 \leq p \leq 1$; the result is $\ln \frac{1+\sqrt{1+4p^2}}{2}$, which for $p = 1/2$ identifies with the complexity found in the $R \to 0$ limit of the present approach.

In Figure 2, we plot the projection of the annealed complexity with fixed magnetization $\Sigma_A(m, H)$ onto the $H - m$ plane for $R = 2$. Only the region where the complexity is positive is shown: this is the region where the number of metastable states is exponentially large and thus comparable to the total number of states in the system; in the rest of the plane, $\Sigma_A(m, H) < 0$, and the number of metastable states is equal to zero in the thermodynamic limit. Several curves in Figure 2 are of special interest: i) the contour $\Sigma_A(m, H) = 0$, ii) the curve $m_A(H)$ which is the locus of the maxima of $\Sigma_A(m, H)$ and thus gives the magnetization of the metastable states dominating the (unrestricted) average number $\overline{\mathcal{N}(H)}$ in the thermodynamic limit (i.e. $\Sigma_A^{max}(H) \equiv \Sigma_A(m_A(H), H)$), and iii) the $T = 0$ saturation hysteresis loop calculated in reference [3] from probabilistic arguments. We see on this example that the contour $\Sigma_A(m, H) = 0$ significantly overestimates the size of the actual hysteresis loop (a similar observation was made in the case of the Sherrington-Kirkpatrick model [10]). The fact that the saturation loop lies well inside the contour $\Sigma_A(m, H) = 0$ can be understood as follows. Each realization of the disorder has a different saturation loop and, as shown in Appendix A, there are no metastable states outside that loop. However, the observed saturation loop is obtained by averaging the magnetization over all disorder realizations, an averaging which is dominated by the *typical* realizations and as such is related to the quenched complexity $\Sigma_Q(m, H)$ that from Jensen's inequality is always less than $\Sigma_A(m, H)$. So,
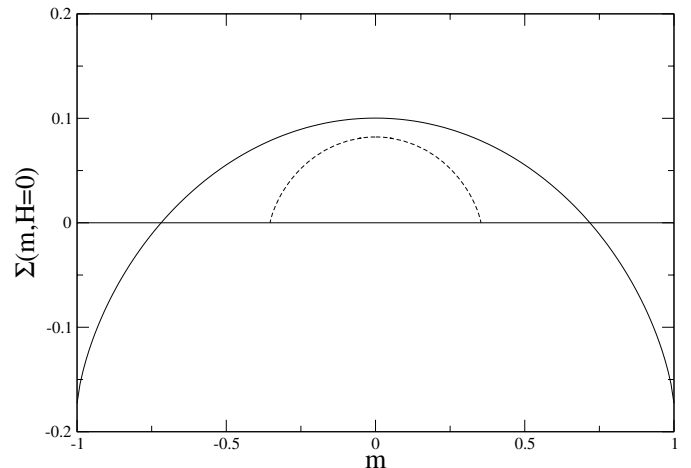
metastable states do exist outside the (average) saturation loop, there may even exist an exponentially large number of them, but these states are *non-typical* and essentially non-observable.

4.2 Quenched complexity

As discussed in Section 3 and Appendix B, the quenched complexity and the magnetization are parameterized by g (see, e.g., Eq. (38)), with the maximum number of metastable states corresponding to $g = 0$. As g goes from 0 to $+\infty$ (resp. $-\infty$), $\Sigma_Q(g, H)$ decreases monotonically towards 0 whereas $m(g, H)$ increases (resp. decreases) monotonically, the surface $\Sigma_Q(m, H)$ having roughly the same overall shape as $\Sigma_A(m, H)$: this is illustrated in Figure 3 for $R = 2$. Note however that the derivative $\partial \Sigma(m, H)/\partial m$, i.e., the value of g, becomes infinite for nontrivial values of the magnetization for the quenched complexity whereas this only occurs for $m = +1$ or -1 for the annealed complexity.

The projection of $\Sigma_Q(m, H)$ onto the $H - m$ plane is shown in Figure 4 for $R = 2$, together with $m(g = 0, H)$, the typical magnetization of the metastable states [24]. The region where $\Sigma_Q(m, H)$ is positive is clearly thinner than the corresponding region for $\Sigma_A(m, H)$ shown in Figure 2. In fact, as proven analytically in Appendix C, the contour $\Sigma_Q(m, H) = 0$ obtained in the limit $g \to \pm\infty$ corresponds *exactly* to the saturation loop calculated in reference [3]. This means that the $T = 0$ hysteresis loop is indeed the envelope of *all* the typical metastable states in the thermodynamic limit (i.e. the entropy density is strictly positive everywhere inside the loop).

We show in Figure 5 the total quenched complexity in zero field $\Sigma_Q^{max}(H = 0)$, which is equal to $\Sigma_Q(m = 0, H = 0)$, as a function of R. It can be seen that the curve is very flat near $R = 0$ and that $\lim_{R \to 0} \Sigma_Q^{max}(H = 0) \approx 0.179$ (see Appendix C), which differs from the limit of the
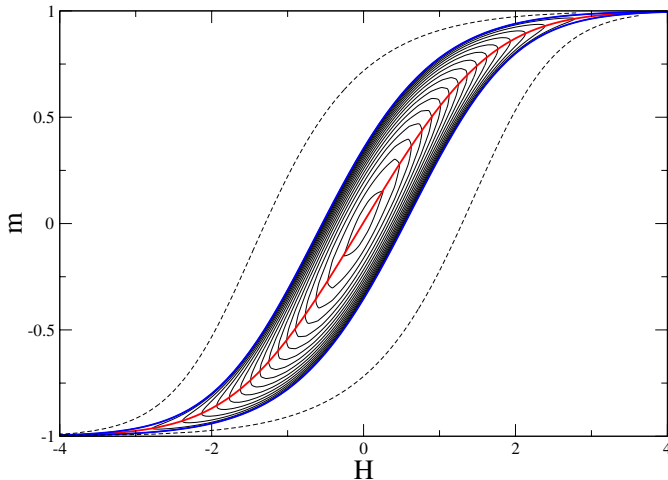
Fig. 4. (Color online) Projection of $\Sigma_Q(m, H)$ onto the $H - m$ plane for $z = 2$ and $R = 2$. The contours are separated by 5×10^{-3} (with $\Sigma_Q(0, 0) \approx 0.082$). The contour $\Sigma_Q(m, H) = 0$ (in blue) coincides with the saturation hysteresis loop calculated in reference [3], as shown in Appendix C. The dashed curve is the annealed contour $\Sigma_A(m, H) = 0$. The red curve is the typical magnetization of the metastable states (the locus of the maxima of the quenched complexity).
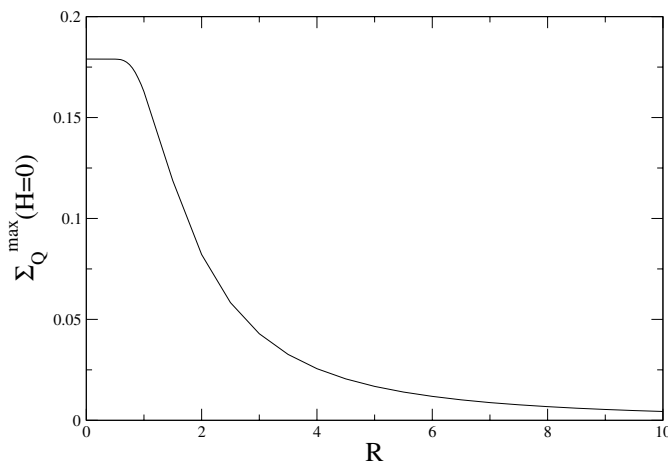

Fig. 5. Total quenched complexity in zero field $\Sigma_Q^{max}(H = 0)$ for $z = 2$ as a function of disorder strength.

annealed complexity $\lim_{R \to 0} \Sigma_A^{max}(H = 0) = \ln \frac{1+\sqrt{2}}{2} \approx 0.188$ (the difference is well outside the error bars in the numerics), itself smaller than the total complexity of the pure system. As discussed above in commenting the latter result, those differences come from the singular features of the limit $R \to 0$: when $R \neq 0$, no metastable states are marginal, whereas when $R = 0$ all metastable states are marginal. However, contrary to what happens for the annealed complexity in the limit $R \to 0$, the present procedure for calculating the quenched complexity does not reduce to a simple (and biased) way of counting the marginal states in the pure system. (Note also that $\Sigma_Q^{max}(H = 0) \approx 0.176$ for $R = 0.75$, which is at odds with the value $\Sigma_Q^{max}(H = 0) \approx 0.25$ that can be extracted from the Figure 5 of Ref. [18]; this latter result is actually

larger than the corresponding annealed complexity obtained from equation (39), $\Sigma_A^{max}(H = 0) \approx 0.186$, which clearly violates Jensen's inequality and suggests some flaw in the calculations of Ref. [18].)

5 Annealed complexity for $z > 2$

For $z > 2$ one expects new phenomena to take place. In particular, the complexity may not be anymore a convex function of H and m and phase transitions may occur.

Let us first consider the case $z = 3$. In Figure 6 we show $\Sigma_A(m, H)$ as a function of the magnetization for two different values of R and several values of the external field (we only consider positive values of H because of the symmetry $\Sigma(m, -H) = \Sigma(-m, H)$). As can be seen in the left panel of the figure, the complexity is always a convex function of the magnetization when R is large enough. As a consequence, the total complexity $\Sigma_A^{max}(H) = \max_m \Sigma_A(m, H)$ is a continuous function of H, as shown in Figure 7. This is also the case for the corresponding magnetization $m_A(H)$. There are only two values of m for which $\Sigma_A(m, H) = 0$ (note that the two limiting values $\lim_{m \to \pm 1} \Sigma_A(m, H) = \ln[(1 + \text{erf}[(zJ \pm H)/(R\sqrt{2})])/2]$ are negative), and the overall surface $\Sigma_A(m, H)$ has roughly the same shape as for $z = 2$ (the projection onto the $H - m$ plane resembles the one shown in Fig. 2).

The behavior is more complicated at low disorder as illustrated by the curves in the right panel of Figure 6. For R smaller than some critical value ($R \lesssim 1.28$) and in a certain range of H, $\Sigma_A(m, H)$ may indeed display two positive maxima at two distinct values of m. As a consequence, there is a discontinuity in $\partial \Sigma_A^{max}(H)/\partial H$ at some value of the field ($H \approx 1.355$ for $R = 1.2$) as shown in Figure 7 and, accordingly, there is a jump in $m_A(H)$. Moreover, for R even smaller, there is a small range of H for which $\Sigma_A(m, H) = 0$ for four distinct values of the magnetization. This yields an overall surface $\Sigma_A(m, H)$ that has a more complicated shape than in the strong-disorder regime, as illustrated by the projection onto the $H - m$ plane shown in Figure 8. In particular, one can observe in the right panel the "S" shape of the contour $\Sigma_A(m, H) = 0$ in the range $1.3 < H < 1.4$. Note that the actual hysteresis loop calculated in reference [4] is again inside the contour $\Sigma_A(m, H) = 0$ as it must be. The fact that $\partial m_A(H)/\partial H$ is negative in a certain range of H is surprising and can possibly be explained by the existence of metastable states that have a quite non-typical magnetization. One must recall, however, that $m_A(H)$ is not an observable quantity. For the same reason, the non-monotonic behavior associated with the contour $\Sigma_A(m, H) = 0$ bears no connection with the behavior of the actual hysteresis loop: this latter does not display any finite jump nor phase transition for $z = 3$ [4].

For $z = 4$, the situation changes for the hysteresis: a phase transition and a jump discontinuity appear for $R \lesssim 1.78$ [4]. $\Sigma_A(m, H)$, on the other hand, has the same type of behavior as for $z = 3$. In particular, for $R \lesssim 2.25$ and in
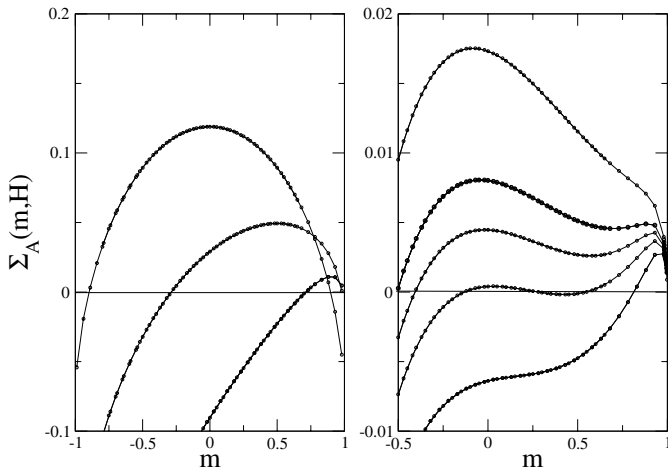
Fig. 6. Annealed complexity $\Sigma_A(m, H)$ for $z = 3$ as a function of m for different values of H. Left panel: $R = 2$; from top to bottom $H = 0, 1.30, 2$. Right panel: $R = 1.2$; from top to bottom $H = 1.30, 1.34, 1.355, 1.372, 1.40$ (the values of $\Sigma_A(m = 1, H)$ not visible here are slightly negative).
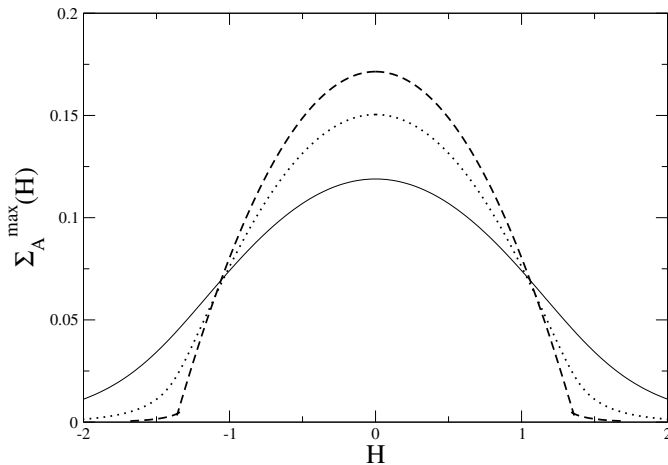

Fig. 7. Total annealed complexity $\Sigma_A^{max}(H)$ for $z = 3$ and $R = 2$ (solid line), 1.5 (dotted line), and 1.2 (dashed line). Note the discontinuity in the slope of $\Sigma_A^{max}(H)$ at $H \approx 1.355$ for $R = 1.2$.

a certain range of the external field H, it has two positive maxima as a function of m and four zeros, like in the left panel of Figure 6. The projection of $\Sigma_A(m, H)$ onto the $H - m$ plane is shown in Figure 9 for $R = 1.5$. $m_A(H)$ has again a strange behavior, first decreasing (resp. increasing) as H is increased (resp. decreased) and then jumping to a value which is very close to 1 (resp. -1). This is probably the generic behavior for $z \geq 4$.

6 Discussion

One important conclusion of the computations presented above is that the annealed approximation does not properly describe the actual distribution of the metastable states of the RFIM in the field-magnetization diagram (i.e., the distribution of metastable states associated with
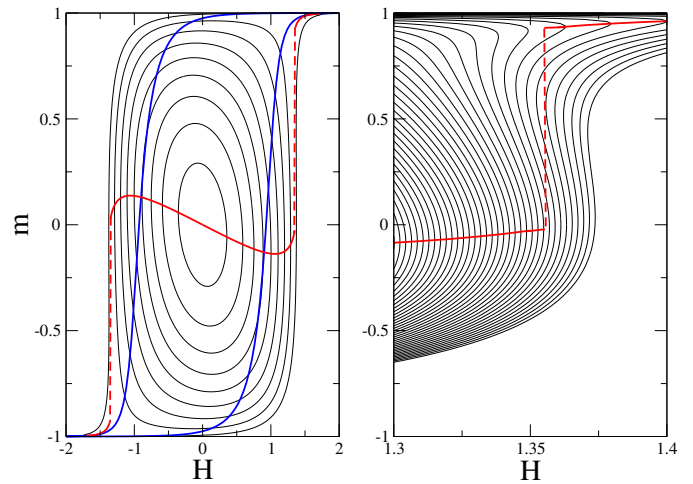

Fig. 8. (Color on line) Projection of $\Sigma_A(m, H)$ onto the $H - m$ plane for $z = 3$ and $R = 1.2$. In the left panel, the contours are separated by 2×10^{-2} (with $\Sigma_A(0, 0) \approx 0.171$). The red curve is the locus $m_A(H)$ of the maxima of $\Sigma_A(m, H)$. The blue curve is the $T = 0$ hysteresis loop calculated in reference [4]. The right panel is a close-up of the figure in the range $1.3 < H < 1.4$, with a spacing 5×10^{-4} between the contours.
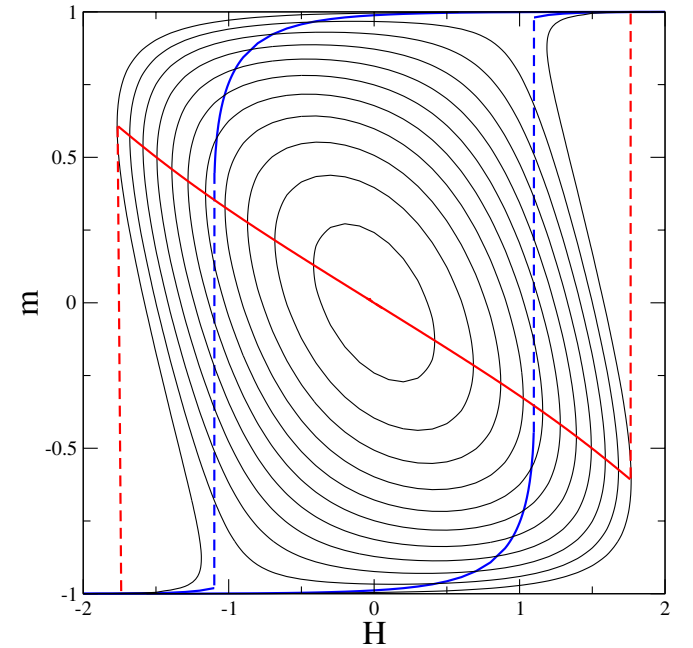
Fig. 9. (Color on line) Projection of $\Sigma_A(m, H)$ onto the $H - m$ plane for $z = 4$ and $R = 1.5$. The contours are separated by 1.5×10^{-2} (with $\Sigma_A(0, 0) \approx 0.159$). The red curve is the locus $m_A(H)$ of the maxima of $\Sigma_A(m, H)$. The blue curve is the $T = 0$ hysteresis loop calculated in reference [4].

typical realizations of the disorder). The calculations are done here on a Bethe lattice, but this conclusion is probably true for any lattice. Predictions can even be qualitatively wrong, as illustrated by the fact that a phase transition corresponding to a change of convexity of the annealed complexity occurs for $z = 3$ whereas the typical behavior changes for $z \geq 4$ only. On the other hand, the

Fig. 10. (Color on line) Speculative distribution of the metastable and H-states in the $H - m$ plane for $z \geq 4$ in the weak-disorder regime where the hysteresis loop has a jump at $H = \pm H_2$. The number of metastable states i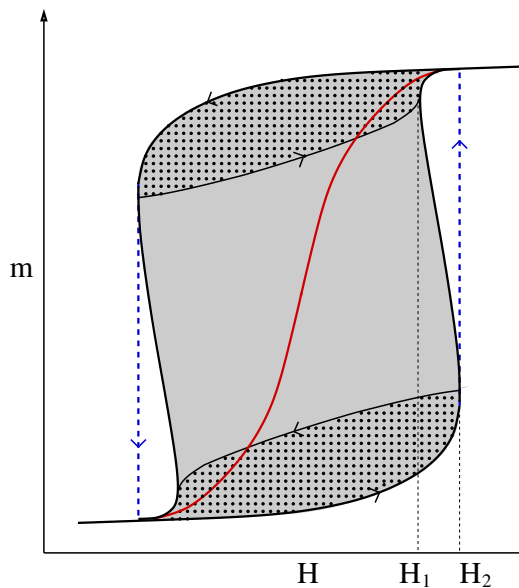s exponentially large in system size in the shaded region and zero outside. Dots indicate the region where the number of H-states is exponentially large. The red curve is the typical magnetization of the metastable states.

quenched calculation for $z = 2$ shows that the entropy density associated to the metastable states is strictly positive everywhere inside the saturation hysteresis loop. It is very likely to be always the case in the strong-disorder regime where the saturation loop is continuous. The situation is less clear for $z \geq 4$ in the weak-disorder regime where the saturation loop displays a jump discontinuity in the magnetization. Since we have not so far been able to carry out the quenched calculation to the end, we can only speculate about the actual behavior of the quenched complexity $\Sigma_Q(m, H)$. A possible scenario is depicted in Figure 10. The rationale for this scenario is very intuitive: we simply assume that the jump in the magnetization curve at some field $H_2(R)$ (or, symmetrically, at $-H_2(R)$) occurs because, with probability 1 in the thermodynamic limit, there are no metastable states with a low magnetization for $H > H_2$. The "S" shape of the curve $\Sigma_Q(m, H) = 0$ is speculative but it is tempting to associate this contour with the real but "unphysical" roots of the self-consistent polynomial equation for the fixed-point probability P^* derived in reference [4] to describe the saturation hysteresis loop. Let us recall that for $z = 4$ this equation has three real solutions in the range $H_1 < H < H_2$ with two of them merging and becoming complex at $H = H_1$ and $H = H_2$. Of course, one cannot discard a more complicated scenario to occur, in particular when there are more than three roots for $z > 4$. In principle, there is also no objection for the existence of a jump discontinuity in the typical magnetization, i.e., the magnetization of the states correspond-

ing to $\max_m \Sigma_Q(m, H)$ (which is not the case considered in Fig. 10). One could indeed imagine a mechanism similar to the one displayed in Figure 6 with $\Sigma_Q(m, H)$ having two maxima as a function of m in a certain range of H: a "first-order" transition could then occur when the two maxima have the same height. These are interesting open questions which remain to be resolved before the problem of the distribution of metastable states of the RFIM on the Bethe lattice can be considered as fully understood. It would be of course even more interesting to know the actual behavior on a 3d lattice, but this can only be done numerically.

Finally, let us remark that very little is known about a special category of metastable states, the so-called "H-states" [26], which are the spin configurations that can be reached by a field history starting from one of the saturated states (these configurations are characterized by the applied sequence of reversal fields $\{H_i\}$). The H-states are thus experimentally observable by recording various hysteresis loops and subloops. The most easily accessible ones, which we have discussed in this paper, are those associated with the saturation hysteresis loop. The H-states are believed to be low-energy configurations, and it has been recently suggested that their number also increases exponentially with the system size [26]. An analytical check of this result would be much welcome, even in one dimension. As was pointed out in introduction, in the weak-disorder regime, for $z \geq 4$, a region around the origin in the $(H - m)$ plane becomes inaccessible to any field history, which forbids a demagnetization process to be completed [12]. The corresponding distribution of the H-states is likely as illustrated in Figure 10. In particular, the probability of finding H-states in the central part of the loop (the region of the $(H - m)$ plane without dots) is zero in the thermodynamic limit. This is related to the fact that the states on the concave parts of the envelope of the shaded region are not reachable by any field history because of the jump in the major hysteresis loop [27].

Appendix A

In this appendix, we show that the probability to find metastable states outside the saturation hysteresis loop vanishes in the thermodynamic limit when the interactions are ferromagnetic. This results from the fact that for any given realization of the random fields, there can be no metastable states outside the corresponding saturation hysteresis loop. Indeed, the properties of the $T = 0$ single-spin-flip dynamics are such that for any given value of the magnetic field H, all sequences starting from the fully polarized configuration (with all spins up or all spins down), sequences in which unstable spins are flipped, lead to the same metastable state on the upper (resp. lower)

branch of the hysteresis loop [1]. This is true in particular for a parallel updating of all unstable spins. Let us denote $\mathcal{C}_\alpha(\mathcal{H})$, $\alpha = 1, ..., p$, the p configurations obtained after each updating steps along this process with $\mathcal{C}_0(H)$ being the initial fully polarized state with, say, all spins up and $\mathcal{C}_p(H) = \mathcal{C}_+(H)$ the final state on the upper branch of the hysteresis loop. The magnetization of course decreases as α increases. Consider now a metastable configuration $\mathcal{C}(\mathcal{H})$. Because of the ferromagnetic nature of the couplings, the unstable spins that flip from $\mathcal{C}_0$ to $\mathcal{C}_1$ must be down in $\mathcal{C}(H)$; the same is true for the unstable spins that flip between $\mathcal{C}_1$ and $\mathcal{C}_2$ and the reasoning can be repeated so that all down spins in $\mathcal{C}_p(H) = \mathcal{C}_+(H)$ must also be down in $\mathcal{C}(\mathcal{H})$. The magnetization of $\mathcal{C}(\mathcal{H})$ is thus less than that of $\mathcal{C}_+(H)$. This is a form of the "no-passing rule" [1]. The argument also applies when starting from the fully polarized state with all spins down, which completes the demonstration. As the property is true for all realizations of the disorder, this applies in particular to the "typical" realizations whose number dominates the whole distribution, so that one expects no "typical" metastable states outside the (average) saturation hysteresis loop.

Appendix B

In this Appendix, we detail the calculation of the quenched complexity for $z = 2$.

Injecting (35) into equation (34), we get the following equations,

$$\frac{e^\Lambda}{\gamma} A = \frac{1-a}{2} e^{-gn} \big[A + Be^{-gn} + C + D(-\mathbf{1}, -\mathbf{1})$$
$$+ \sum_{\boldsymbol{\tau}_1} E(\boldsymbol{\tau}_1, -\mathbf{1}) \big] + \frac{a-b}{2} e^{-gn} A \quad \text{(B1a)}$$

$$\frac{e^\Lambda}{\gamma} C = \frac{1-c}{2} e^{-gn} \big[A + Be^{-gn} + C + E(\mathbf{1}, \mathbf{1})$$
$$+ \sum_{\boldsymbol{\tau}_1} D(\boldsymbol{\tau}_1, \mathbf{1}) \big] + \frac{b+c}{2} e^{-gn} C \quad \text{(B1b)}$$

$$\frac{e^\Lambda}{\gamma} B = \frac{a-b}{2} C + \frac{b+c}{2} A \quad \text{(B1c)}$$

and

$$\frac{e^\Lambda}{\gamma} D(\boldsymbol{\sigma}, \boldsymbol{\tau}) = \frac{a-b}{2} e^{gs} \Big\{ Be^{gs} + D(\boldsymbol{\sigma}, \boldsymbol{\sigma}) + \sum_{\boldsymbol{\tau}_1} E(\boldsymbol{\tau}_1, \boldsymbol{\sigma})$$
$$\times \prod_a \big[\delta(\sigma^a; -1)\delta(\tau_1^a; -\tau^a)$$
$$+ \delta(\tau_1^a; \tau^a)\delta(\tau^a; \sigma^a) \big] \Big\} \quad \text{(B2a)}$$

$$\frac{e^\Lambda}{\gamma} E(\boldsymbol{\sigma}, \boldsymbol{\tau}) = \frac{b+c}{2} e^{gs} \Big\{ Be^{gs} + E(\boldsymbol{\sigma}, \boldsymbol{\sigma}) + \sum_{\boldsymbol{\tau}_1} D(\boldsymbol{\tau}_1, \boldsymbol{\sigma})$$
$$\times \prod_a \big[\delta(\sigma^a; 1)\delta(\tau_1^a; -\tau^a) + \delta(\tau_1^a; \tau^a)\delta(\tau^a; \sigma^a) \big] \Big\}. \quad \text{(B2b)}$$

After some algebra we also obtain from equation (21) the additional equation

$$(A + C)^2 + 2B(Ae^{-gn} + Ce^{gn}) + B^2(2\cosh 2g)^n$$
$$+ 2B \sum_{\boldsymbol{\sigma}} e^{gs}[D(\boldsymbol{\sigma}, \boldsymbol{\sigma}) + E(\boldsymbol{\sigma}, \boldsymbol{\sigma})] + 2A[D(-\mathbf{1}, -\mathbf{1})$$
$$+ \sum_{\boldsymbol{\tau}} E(\boldsymbol{\tau}, -\mathbf{1})] + 2C[E(\mathbf{1}, \mathbf{1}) + \sum_{\boldsymbol{\tau}} D(\boldsymbol{\tau}, \mathbf{1})]$$
$$+ \sum_{\boldsymbol{\sigma}}[D^2(\boldsymbol{\sigma}, \boldsymbol{\sigma}) + E^2(\boldsymbol{\sigma}, \boldsymbol{\sigma})] + 2\sum_{\boldsymbol{\sigma}, \boldsymbol{\tau}} D(\boldsymbol{\sigma}, \boldsymbol{\tau})E(\boldsymbol{\tau}, \boldsymbol{\sigma})$$
$$\times \prod_a [\delta(\sigma^a; 1)\delta(\tau^a; -1) + \delta(\sigma^a; \tau^a)] = 1. \quad \text{(B3)}$$

Equations (B1–B3) constitute a set of six coupled equations that must be solved at the first two orders in n. As already mentioned after equation (35), it is important to note that $D(\boldsymbol{\sigma}, \boldsymbol{\tau})$ and $E(\boldsymbol{\sigma}, \boldsymbol{\tau})$ are functions of two variables only. Indeed, the term $\prod_a \big[\delta(\sigma^a; -1))\delta(\tau^a; 1) + \delta(\tau^a; \sigma^a)\big]$ in equation (36) imposes that $\sigma^a = 1$ and $\tau^a = -1$ cannot hold simultaneously. This in turns implies that $u = n - |s - t|$.

We now expand both sides of equations (B1–B3) at order n. Let us first consider objects like $D(-\mathbf{1}, -\mathbf{1}), \sum_{\boldsymbol{\tau}_1} D(\boldsymbol{\tau}_1, \mathbf{1})$, etc... in equations (B1). Using the integral representations (37) of $D(\boldsymbol{\sigma}, \boldsymbol{\tau})$ and $E(\boldsymbol{\sigma}, \boldsymbol{\tau})$, we find

$$D(-\mathbf{1}, -\mathbf{1}) = \int dxdy \hat{D}(x, y)e^{-n(x+y)}$$
$$= D_0 + n(D_1 - S_1 - S_2) + O(n^2) \quad \text{(B4)}$$

$$\sum_{\boldsymbol{\tau}_1} D(\boldsymbol{\tau}_1, \mathbf{1}) = \int dxdy \hat{D}(x, y)e^{ny} \sum_{\boldsymbol{\tau}_1} e^{x \sum_a \tau_1^a}$$
$$= D_0 + n(D_1 + S_2 + S_3) + O(n^2) \quad \text{(B5)}$$

where $D_0 = \int dxdy \hat{D}_0(x, y)$, $D_1 = \int dxdy \hat{D}_1(x, y)$, $S_1 = \int dxdy x \hat{D}_0(x, y)$, $S_2 = \int dxdy y \hat{D}_0(x, y)$, and $S_3 = \int dxdy \hat{D}_0(x, y) \ln[2 \cosh x]$. (Similar expressions are obtained for $E(\mathbf{1}, \mathbf{1})$ and $\sum_{\boldsymbol{\tau}_1} E(\boldsymbol{\tau}_1, \text{-}\mathbf{1})$, with E_0, E_1, S_1', S_2' and S_3' replacing respectively $D_0, D_1, -S_1, -S_2$ and S_3.)

In the same way, one has in equation (B3)

$$\sum_{\boldsymbol{\sigma}} e^{gs}[D(\boldsymbol{\sigma}, \boldsymbol{\sigma}) + E(\boldsymbol{\sigma}, \boldsymbol{\sigma})] =$$
$$\int dxdy[\hat{D}(x, y) + \hat{E}(x, y)] \sum_{\boldsymbol{\sigma}} e^{s(g+x+y)}$$
$$= D_0 + E_0 + n(D_1 + E_1 + S_4) + O(n^2) \quad \text{(B6)}$$

$$\sum_{\boldsymbol{\sigma}}[D^2(\boldsymbol{\sigma},\boldsymbol{\sigma}) + E^2(\boldsymbol{\sigma},\boldsymbol{\sigma})] = \int dxdydx'dy'$$

$$\times [\hat{D}(x,y)\hat{D}(x',y') + \hat{E}(x,y)\hat{E}(x',y')]\sum_{\boldsymbol{\sigma}} e^{s(x+y+x'+y')}$$

$$= D_0^2 + E_0^2 + n(2D_0D_1 + 2E_0E_1 + S_5) + O(n^2) \quad \text{(B7)}$$

$$\sum_{\boldsymbol{\sigma},\boldsymbol{\tau}} D(\boldsymbol{\sigma},\boldsymbol{\tau})E(\boldsymbol{\tau},\boldsymbol{\sigma})\prod_a[\delta(\sigma^a;-1)\delta(\tau^a;1) + \delta(\sigma^a;\tau^a)] =$$

$$\int dxdydx'dy'\hat{D}(x,y)\hat{E}(x',y')\sum_{\boldsymbol{\sigma},\boldsymbol{\tau}} e^{s(x+y')+t(y+x')}$$

$$\times \prod_a[\delta(\sigma^a;-1)\delta(\tau^a;1) + \delta(\sigma^a;\tau^a)]$$

$$= D_0E_0 + n(D_0E_1 + D_1E_0 + S_6) + O(n^2) \quad \text{(B8)}$$

where $S_4 = \int dxdy[\hat{D}_0(x,y) + \hat{E}_0(x,y)]\ln[2\cosh(x + y + g)]$, $S_5 = \int dxdydx'dy'[\hat{D}_0(x,y)\hat{D}_0(x',y') + \hat{E}_0(x,y)\hat{E}_0(x',y')]\ln[2\cosh(x + y + x' + y')]$ and $S_6 = \int dxdydx'dy'\hat{D}_0(x,y)\hat{E}_0(x',y')\ln[e^{-x+y+x'-y'} + 2\cosh(x + y + x' + y')]$.

The treatment of equations (B2) is slightly more involved. Consider first the term $T = e^{gs}\sum_{\boldsymbol{\tau}_1} E(\boldsymbol{\tau}_1,\boldsymbol{\sigma})\times \prod_a\left[\delta(\sigma^a;-1)\delta(\tau_1^a;-\tau^a) + \delta(\tau_1^a;\tau^a)\delta(\tau^a;\sigma^a)\right]$ in equation (B2a). Performing the sum over $\boldsymbol{\tau}_1$ gives $T = \int dxdy\hat{E}(x,y)\prod_a f_{\sigma^a\tau^a}(x,y)$ with

$$f_{\sigma^a\tau^a}(x,y) = e^{-x\tau^a-y-g}\delta(\sigma^a;-1) + e^{(x+y+g)\sigma^a}\delta(\sigma^a;\tau^a). \quad \text{(B9)}$$

Following reference [15], we now use the identity

$$\prod_a f_{\sigma^a\tau^a} = \exp[\sum_a \ln f_{\sigma^a\tau^a}]$$

$$= \exp\left[\sum_a\sum_{\sigma,\tau}\delta(\sigma;\sigma^a)\delta(\tau;\tau^a)\ln f_{\sigma\tau}\right] \quad \text{(B10)}$$

with

$$\sum_a \delta(\sigma;\sigma^a)\delta(\tau;\tau^a) =$$

$$\begin{cases} \frac{1}{4}(s + u + t + n) & \text{for } \sigma = \tau = 1 \\ \frac{1}{4}(s - u - t + n) & \text{for } \sigma = 1, \tau = -1 \\ \frac{1}{4}(-s - u + t + n) & \text{for } \sigma = -1, \tau = 1 \\ \frac{1}{4}(-s + u - t + n) & \text{for } \sigma = \tau = -1 . \end{cases}$$

Remembering that the combination $\sigma^a = 1, \tau^a = -1$ is forbidden and that $u = n + s - t$, we then obtain

$$\prod_a f_{\sigma^a\tau^a}(x,y) = \exp\left[\frac{s+n}{2}\ln f_{++}(x,y) + \frac{t-s}{2}\ln f_{-+}(x,y) - \frac{t-n}{2}\ln f_{--}(x,y)\right] \quad \text{(B11)}$$

with $f_{++}(x,y) = e^{x+y+g}$, $f_{-+}(x,y) = e^{-(x+y+g)}$ and $f_{--}(x,y) = e^{x-y-g} + e^{-(x+y+g)}$. Hence

$$T = \int dxdy\hat{E}(x,y)\exp\Big[s(x + y + g) - \frac{t}{2}\ln\left(1 + e^{2x}\right) + \frac{n}{2}\ln\left(1 + e^{2x}\right)\Big]. \quad \text{(B12)}$$

Using the same procedure, we get

$$e^{gs}D(\boldsymbol{\sigma},\boldsymbol{\sigma}) = \int dxdy\hat{D}(x,y)\exp[s(x + y + g)]. \quad \text{(B13)}$$

Finally, Fourier transforming both sides of equation (B2a) with respect to s and t, we obtain

$$\frac{e^\Lambda}{\gamma}\hat{D}(x,y) = \frac{a-b}{2}\bigg\{ B\delta(x - 2g)\delta(y) + \delta(y)$$

$$\times \int dx'\hat{D}\left(x', x - x' - g\right)$$

$$+ \int dx'dy'\hat{E}\left(x',y'\right)\delta\left(x - x' - y' - g\right)$$

$$\times \delta\left(y + \frac{1}{2}\ln\left[1 + e^{2x'}\right]\right)e^{\frac{n}{2}\ln\left(1+e^{2x'}\right)}\bigg\}. \quad \text{(B14)}$$

In the same way, the Fourier transform of equation (B2b) gives

$$\frac{e^\Lambda}{\gamma}\hat{E}(x,y) = \frac{b+c}{2}\bigg\{ B\delta(x - 2g)\delta(y) + \delta(y)$$

$$\times \int dx'\hat{E}(x', x - x' - g)$$

$$+ \int dx'dy'\hat{D}(x',y')\delta(x - x' - y' - g)$$

$$\times \delta\left(y - \frac{1}{2}\ln\left[1 + e^{-2x'}\right]\right)e^{\frac{n}{2}\ln\left(1-e^{2x'}\right)}\bigg\}. \quad \text{(B15)}$$

Collecting all terms at order n^0, we obtain the six coupled equations

$$\frac{e^{\Lambda_0}}{\gamma}A_0 = \frac{1-a}{2}\left[A_0 + B_0 + C_0 + D_0 + E_0\right] + \frac{a-b}{2}A_0 \quad \text{(B16a)}$$

$$\frac{e^{\Lambda_0}}{\gamma}C_0 = \frac{1-c}{2}\left[A_0 + B_0 + C_0 + D_0 + E_0\right] + \frac{b+c}{2}C_0 \quad \text{(B16b)}$$

$$\frac{e^{\Lambda_0}}{\gamma}B_0 = \frac{a-b}{2}C_0 + \frac{b+c}{2}A_0 \quad \text{(B16c)}$$

$$\hat{D}_0(x,y) = \frac{a-b}{2}\bigg\{ B_0\delta(x - 2g)\delta(y) + \delta(y)$$

$$\times \int dx'\hat{D}_0(x', x - x' - g)$$

$$+ \int dx'dy'\hat{E}_0(x',y')\delta(x - x' - y' - g)$$

$$\times \delta\left(y + \frac{1}{2}\ln\left[1 + e^{2x'}\right]\right)\bigg\} \quad \text{(B17a)}$$

$$\hat{E}_0(x,y) = \frac{b+c}{2}\left\{ B_0\delta(x-2g)\delta(y) + \delta(y)\right.$$

$$\times \int dx'\,\hat{E}_0(x',x-x'-g)$$

$$+ \int dx'dy'\,\hat{D}_0(x',y')\delta(x-x'-y'-g)$$

$$\left.\delta\left(y-\frac{1}{2}\ln\left[1+e^{-2x'}\right]\right)\right\} \qquad \text{(B17b)}$$

and

$$(A_0+B_0+C_0+D_0+E_0)^2 = 1. \qquad \text{(B18)}$$

Equations (B16) and (B18) may be decoupled from equations (B17) by performing the integration of (B17) over x and y which readily gives

$$D_0 = \frac{a-b}{2-(a+c)}B_0, \ E_0 = \frac{b+c}{2-(a+c)}B_0. \qquad \text{(B19)}$$

The only physical solution of equations (B16), (B18) and (B19) is then

$$\Lambda_0 = \ln\gamma \qquad \text{(B20a)}$$

$$A_0 = \frac{1-a}{2-(a-b)} \qquad \text{(B20b)}$$

$$B_0 = \frac{(a-b)(1-c)}{4-2(b+c)} + \frac{(b+c)(1-a)}{4-2(a-b)} \qquad \text{(B20c)}$$

$$C_0 = \frac{1-c}{2-(b+c)}. \qquad \text{(B20d)}$$

Note that equation (B20) is necessary for the $n \to 0$ limit to exist when $z = 2$ (as pointed out after Eq. (30)). This solution corresponds to the choice $A_0+B_0+C_0+D_0+E_0 = 1$ in equation (B18) which implies that $\lim_{n\to 0}\sum_{\boldsymbol{\sigma},\boldsymbol{\tau}} c(\boldsymbol{\sigma},\boldsymbol{\tau}) = \sqrt{2/\gamma}$, a result that could have been also obtained from equation (21) by naively (but incorrectly) using a Fourier integral representation of $c(\boldsymbol{\sigma},\boldsymbol{\tau})$.

It remains to solve the coupled integral equations (B17). This can be done by writting formally $\hat{D}_0(x,y)$ and $\hat{E}_0(x,y)$ as two infinite series of delta functions. The locations of the peaks are then obtained recursively as discussed in Appendix C.

We now achieve the calculation of the quenched complexity by solving equations (B1–B3) at first order in n. Using equations (B4–B8), (B14–B15), (B17–B18), and (B20a), we obtain, after some manipulations,

$$\left[\Lambda_1+\frac{1-b}{2}g\right]A_0 + \frac{1+b}{2}A_1 =$$

$$\frac{1-a}{2}\left[-g(C_0+2B_0+D_0+E_0)\right.$$

$$+ C_1+B_1+D_1+E1$$

$$\left. - S1-S2+S_3'-S_2'\right] \qquad \text{(B21a)}$$

$$\left[\Lambda_1-\frac{1-b}{2}g\right]C_0 + \frac{1-b}{2}C_1 = \frac{1-c}{2}\left[g(A_0+2B_0+D_0+E_0)\right.$$

$$+ A_1+B_1+D_1+E_1$$

$$\left. + S_1'+S_2'+S_3+S_2\right] \qquad \text{(B21b)}$$

$$\Lambda_1 B_0 + B_1 = \frac{a-b}{2}C_1 + \frac{b+c}{2}A_1 \qquad \text{(B21c)}$$

$$\hat{D}_1(x,y) = -(y+\Lambda_1)\hat{D}_0(x,y)$$

$$+ \frac{a-b}{2}\left\{ B_1\delta(x-2g)\delta(y) + \delta(y)\int dx'\,\hat{D}_1(x',x-x'-g)\right.$$

$$+ \int dx'dy'\,\hat{E}_1(x',y')$$

$$\left.\times \delta(x-x'-y'-g)\delta\left(y+\frac{1}{2}\ln\left[1+e^{2x'}\right]\right)\right\} \qquad \text{(B22a)}$$

$$\hat{E}_1(x,y) = (y-\Lambda_1)\hat{E}_0(x,y) + \frac{b+c}{2}\left\{ B_1\delta(x-2g)\delta(y)\right.$$

$$+ \delta(y)\int dx'\,\hat{E}_1(x',x-x'-g)$$

$$+ \int dx'dy'\,\hat{D}_1(x',y')\delta(x-x'-y'-g)$$

$$\left.\times \delta\left(y-\frac{1}{2}\ln\left[1+e^{-2x'}\right]\right)\right\} \qquad \text{(B22b)}$$

$$A_1+B_1+C_1+D_1+E_1+g(C_0-A_0)B_0$$

$$+ \frac{B_0^2}{2}\ln[2\cosh(2g)] + (C_0-A_0)(S_2+S_2')$$

$$+ C_0(S_1'+S_3) + A_0(S_3'-S_1) + B_0S_4 + \frac{S_5}{2} + S_6 = 0. \qquad \text{(B23)}$$

Integrating equations (B22) over x and y we obtain

$$D_1 = \frac{a-b}{2-a-c}(B_1-\Lambda_1 C_0+S_2') - \frac{2-b-c}{2-a-c}(S_2+\Lambda_1 D_0) \qquad \text{(B24a)}$$

$$E_1 = \frac{b+c}{2-a-c}(B_1-\Lambda_1 D_0-S_2) - \frac{2-a+b}{2-a-c}(S_2'-\Lambda_1 D_0) \qquad \text{(B24b)}$$

which again allows to decouple equations (B21) and (B23) from (B22). The solution of the system of linear equations (B21), (B24), and (B23) then yields

$$\Lambda_1(g) = \frac{1}{2}\left\{ g\big[(b-c)A_0 + (a+b)C_0 + (a-c)\right.$$

$$\times (2B_0+D_0+E_0)\big] - S_1(1-a) + S_1'(1-c)$$

$$+ S_2(a-c-2) + S_2'(a-c+2)$$

$$\left. + S_3(1-c) + S_3'(1-a)\right\} \qquad \text{(B25)}$$

which, remarkably, does not depend on the integrals S_4, S_5 and S_6. In fact, it turns out that $\Lambda_1(g)$ can be written in

terms of a single integral of $\hat{D}_0(x,y)$ or $\hat{E}_0(x,y)$ (for instance S_3). Indeed, the analysis of equations (B22) shows that

$$S_1 = \frac{p(2-p-q)}{(1-p-q)(1-p-q+pq)}g, \quad S_1' = \frac{q}{p}S_1 \quad \text{(B26a)}$$

$$S_2 = -\frac{q}{2}(S_1 + S_3), \quad S_2' = \frac{q}{2}(S_3 - S_1) \quad \text{(B26b)}$$

$$S_3' = \frac{q}{p}S_3. \quad \text{(B26c)}$$

with $p = (a-b)/2$ and $q = (b+c)/2$. Inserting (B26) in equation (B25), using equations (B19) and (B20) and the relation $\Sigma_Q(g,H) = \Lambda_1(g) - g\partial\Lambda_1(g)/\partial g$, we finally obtain equation (38).

Note that the magnetisation $m(g)$ in the limit $n \to 0$ only depends on the solution of the saddle-point equations at lowest order. Inserting equation (35) in equation (22) gives after some algebra

$$
\begin{aligned}
m(g) = {}& C_0^2 - A_0^2 + 2B_0(C_0 - A_0) \\
& + 2(C_0E_0 - A_0D_0) + B_0^2 \tanh 2g \\
& + A_0 \int dxdy\,\hat{E}_0(x,y)[\tanh x - 1] \\
& + C_0 \int dxdy\,\hat{D}_0(x,y)[\tanh x + 1] \\
& + 2B_0 \int dxdy[\hat{D}_0(x,y) \\
& + \hat{E}_0(x,y)] \tanh(x+y+g) \\
& + \int dxdydx'dy'[\hat{D}_0(x,y)\hat{D}_0(x',y') \\
& + \hat{E}_0(x,y)\hat{E}_0(x',y')] \tanh(x+y+x'+y') \\
& + 2\int dxdydx'dy'\,\hat{D}_0(x,y)\hat{E}_0(x',y') \\
& \times \frac{e^{x+y+x'+y'} - e^{-(x+y+x'+y')}}{e^{-x+y+x'-y'} + e^{x+y+x'+y'} + e^{-(x+y+x'+y')}}.
\end{aligned}
$$
$$\text{(B27)}$$

Appendix C

The solution of the coupled integral equations (B17) cannot be obtained in the form of closed expressions for $\hat{D}_0(x,y)$ and $\hat{E}_0(x,y)$. However, this type of self-consistent equations is common in one-dimensional disordered systems and it is easy to see that $\hat{D}_0(x,y)$ and $\hat{E}_0(x,y)$ may be represented as two *infinite* series of delta functions which are conveniently written as

$$\hat{D}_0(x,y)/B_0 = p \sum_{i=0}^{\infty} \sum_{j=0}^{i} p^j q^{i-j} \tilde{D}_{ij}(x,y) \quad \text{(C1a)}$$

$$\hat{E}_0(x,y)/B_0 = q \sum_{i=0}^{\infty} \sum_{j=0}^{i} q^j p^{i-j} \tilde{E}_{ij}(x,y) \quad \text{(C1b)}$$

with $p = (a-b)/2$, $q = (b+c)/2$ and

$$\tilde{D}_{ij}(x,y) = \sum_{k=1}^{\binom{i}{j}} \delta\big(x - x_k^{(ij)}(g)\big)\delta\left(y - y_k^{(ij)}(g)\right) \quad \text{(C2a)}$$

$$\tilde{E}_{ij}(x,y) = \sum_{k=1}^{\binom{i}{j}} \delta\left(x - x_k'^{(ij)}(g)\right)\delta\left(y - y_k'^{(ij)}(g)\right). \quad \text{(C2b)}$$

$\tilde{D}_{ij}(x,y)$ and $\tilde{E}_{ij}(x,y)$ are then computed iteratively, the coordinates $(x_k^{(ij)}, y_k^{(ij)})$ and $(x_k'^{(ij)}, y_k'^{(ij)})$ of the delta peaks at step i being obtained from the coordinates at step $i-1$, with $\tilde{D}_{00}(x,y) = \tilde{E}_{00}(x,y) = \delta(x-2g)\delta(y)$. For instance, the first terms in the expansion of $\hat{D}_0(x,y)$ are

$$\tilde{D}_{10}(x,y) = \delta(x-3g)\delta\left(y + \frac{1}{2}\ln\left(1+e^{4g}\right)\right)$$

$$\tilde{D}_{11}(x,y) = \delta(x-3g)\delta(y)$$

$$\tilde{D}_{20}(x,y) = \delta(x-4g)\delta\left(y + \frac{1}{2}\ln\left(1+e^{6g}\right)\right)$$

$$\tilde{D}_{21}(x,y) = \delta\left(x - 4g + \frac{1}{2}\ln\left(1+e^{4g}\right)\right)\delta(y)$$

$$+ \delta\left(x - 4g - \frac{1}{2}\ln(1+e^{-4g})\right)\delta\left(y + \frac{1}{2}\ln\left(1+e^{6g}\right)\right)$$

$$\tilde{D}_{22}(x,y) = \delta(x-4g)\delta(y)$$

etc... $\quad$ (C3)

Note that p and q depend on H and R whereas the dependence on g is only contained in the position of the delta functions. With equation (B1a), the integral S_3 also becomes an infinite series,

$$S_3(g) = B_0 p \sum_{i=0}^{\infty} \sum_{j=0}^{i} p^j q^{i-j} \sum_{k=1}^{\binom{i}{j}} \ln\left[2\cosh x_k^{(ij)}(g)\right]. \quad \text{(C4)}$$

The number of delta functions grows exponentially during the iteration procedure and the precision on S_3 depends on the number I of terms that are included in the infinite sums. However, the cumulative weight of the delta peaks is finite $(D_0/B_0 = p/(1-p-q)$ and $E_0/B_0 = q/(1-p-q))$, and one can take as many terms as needed so as to satisfy a given accuracy defined by $\epsilon = 1 - (1-p-q)\sum_{i=1}^{I}\sum_{j=0}^{i}\binom{i}{j}p^j q^{i-j}$ (see, e.g., Ref. [25] for a similar calculation). When $H = 0$, however, one has $p = q = (1/2)\,\text{erf}(\sqrt{2}J/R)$ and the convergence of the series becomes progressively poorer as the ratio J/R increases and $p, q \to 1/2$. In this case, it is convenient to write $S_3(g)$ as

$$S_3(g) = B_0 \frac{p}{1-2p} s_3^{\infty}(g) + B_0 p \sum_{i=0}^{\infty} p^i \left[s_3^{(i)}(g) - s_3^{\infty}(g)\right]$$
$$\text{(C5)}$$

where $s_3^{(i)}(g) = \sum_{j=0}^{i}\sum_{k=1}^{\binom{i}{j}}\ln[2\cosh x_k^{(ij)}(g)]$ and $s_3^{\infty}(g) = \lim_{i\to\infty} s_3^{(i)}(g)$. For $g = 0$, for instance, one finds

numerically $s_3^\infty(0) \approx 0.716$ and since $B_0 \sim 1 - 2p$ when $R \to 0$, this yields from equation (38) $\lim_{R \to 0} \Sigma_Q^{max}(H = 0) = s_3^\infty(0)/4 \approx 0.179$.

When $g \to \pm\infty$, the expressions of $\hat{D}_0(x,y)$ and $\hat{E}_0(x,y)$ simplify considerably as the positions of the delta peaks concentrate on a few lines in the $x-y$ plane. Specifically, for $g \to +\infty$, one obtains

$$\hat{D}_0(x,y)/B_0 = \sum_{n=2}^{\infty} \left[p^{n-1} \frac{(1-p)(1-q)}{1-p-q} \delta(x-ng)\delta(y) \right.$$
$$\left. + p\tilde{E}(n-1)\delta(x-ng)\delta(y-(1-n)g) \right] \quad (C6a)$$

$$\hat{E}_0(x,y)/B_0 = \sum_{n=2}^{\infty} \tilde{E}(n)\delta(x-ng)\delta(y) \quad (C6b)$$

with

$$\tilde{E}(n) = q\frac{(1-p)(1-q)}{1-p-q} \left[q^{n-2} + p\frac{p^{n-2} - q^{n-2}}{p-q} \right]. \quad (C7)$$

Replacing in equation (B27) gives, after some algebra,

$$m(g \to +\infty) = 1 - 2A_0(1 + B_0 + D_0)$$
$$= 1 - 2p(-H) \quad (C8)$$

with

$$p(-H) = \frac{(a-1)(a+ac-4+b^2-2b-c)}{(2-a+b)^2}$$
$$= p_0\frac{1 + p_0p_2 - p_1^2}{[1 + p_0 - p_1]^2} \quad (C9)$$

where $p_n(-H) = \int_{2(1-n)+H}^{\infty} P(h)dh$ is the probability (introduced in Ref. [3]) that a spin with n neighbors up $(n = 0, 1, 2)$ is up at the field $-H$: $p_0 = (1-a)/2, p_1 = (1-b)/2, p_2 = (1+c)/2$. The magnetization given by equations (C8–C9) is exactly that calculated in reference [3] for the upper branch of the hysteresis loop. By symmetry, the magnetization on the lower branch of the loop is given by $m = 2p(H) - 1$ and corresponds to the limit $g \to -\infty$.

It remains to calculate $\Lambda_1(g,H)$ and $\Sigma_Q(g,H) = \Lambda_1(g,H) - gm = \Lambda_1(g,H) - g\partial\Lambda_1(g,H)/\partial g$ when $g \to \pm\infty$. Inserting equations (C6-C7) in (B25) gives, after some algebra,

$$\Lambda_1(g \to +\infty, H) \sim$$
$$- g\frac{(a^2c - a - 2ac + ab^2 - 2b^2 - 2b + c)}{(2-a+b)^2}, \quad (C10)$$

from which one readily finds that $\Sigma_Q(g \to +\infty, H) = 0$. By symmetry, Σ_Q also vanishes along the lower branch of the hysteresis loop. To illustrate how the cancellation of terms occurs in $\Sigma_Q(g,H)$ in the limit $g \to \pm\infty$, let us give the first terms in the large-R expansion of $\Lambda_1(g,H)$

and $\Sigma_Q(g,H)$:

$$\Lambda_1(g,H) = g\sqrt{\frac{2}{\pi}}\frac{H}{R} + \frac{2J}{\pi R^2}[2gH + J\ln(2\cosh 2g)]$$
$$- \frac{1}{6\pi R^3}\sqrt{\frac{2}{\pi}}\left[\pi gH^3 + 6\pi gHJ^2 - 24gHJ^2 \right.$$
$$\left. + 24J^3\ln(2\cosh 2g) - 24J^3\ln(2\cosh 3g) \right] + O\left(\frac{J^4}{R^4}\right)$$
$$(C11)$$

$$\Sigma_Q(g,H) = \frac{2J^2}{\pi R^2}[\ln(2\cosh 2g) - 2g\tanh 2g]$$
$$+ \frac{4J^3}{\pi R^3}\sqrt{\frac{2}{\pi}}[2g\tanh 2g - \ln(2\cosh 2g)$$
$$+ \ln(2\cosh 3g) - 3g\tanh 3g] + O\left(\frac{J^4}{R^4}\right).$$
$$(C12)$$

Note that $\Sigma_Q(g,H)$ does not depend on H at the first two orders of the expansion.

References

1. J.P. Sethna, K. Dahmen, S. Kartha, J.A. Krumhansl, B.W. Roberts, J.D. Shore, Phys. Rev. Lett. **70**, 3347 (1993)
2. K. Dahmen, J.P. Sethna, Phys. Rev. B **53**, 14872 (1996); O. Perkovic, K. Dahnen, J.P. Sethna, Phys. Rev. B **59**, 6106 (1999)
3. P. Shukla, Physica A **233**, 235 (1996)
4. D. Dhar, P. Shukla, J.P. Sethna, J. Phys. A **30**, 5259 (1997)
5. A. Berger, A. Inomata, J.S. Jiang, J.E. Pearson, S.D. Bader, Phys. Rev. Lett. **85**, 4176 (2000)
6. J. Marcos, E. Vives, Ll. Mañosa, M. Acet, E. Duman, M. Morin, V. Novak, A. Planes, Phys. Rev. B **67**, 224406 (2003)
7. F. Detcheverry, E. Kierlik, M.L. Rosinberg, G. Tarjus, Phys. Rev. E **68**, 061504 (2003); F. Detcheverry, E. Kierlik, M.L. Rosinberg, G. Tarjus, Langmuir **20**, 8006 (2004)
8. D.J. Tulimieri, J. Yoon, M.H.W. Chan, Phys. Rev. Lett. **82**, 121 (1999)
9. In this work, we study the 1-spin-flip stable states whose energy cannot be lowered by the flip of any single spin. The corresponding dynamics consists in aligning each spin with its local field. Generalization to 2-spin-flip stable states and associated dynamics is considered in E. Vives, M.L. Rosinberg, G. Tarjus, Phys. Rev. B (in press), preprint `cond-mat/0411330` (2004)
10. F. Pazmandi, G. Zarand, G. Zimanyi, Phys. Rev. Lett. **83**, 1034 (1999)
11. A.A. Likhachev, preprint `cond-mat/0007504` (2000)
12. F. Colaiori, A. Gabrielli, S. Zapperi, Phys. Rev. B **65**, 224404 (2002)
13. M. Mezard, G. Parisi, Eur. Phys. J. B **20**, 217 (2001)
14. A. Lefèvre, D.S. Dean, Eur. Phys. J. B **21**, 121 (2001)
15. J. Berg, M. Sellito, Phys. Rev. E **65**, 016115 (2001)
16. A. Pagnani, G. Parisi, M. Ratiéville, Phys. Rev. E **67**, 026116 (2003)

17. D.S. Dean, Eur. Phys. J. B **15**, 493 (2000)
18. S. Masui, A.E. Jacobs, C. Wicentowich, B.W. Southern, J. Phys. A **26**, 25 (1993)
19. More precisely, we expect the complexities, as defined below, to be equal. It was checked numerically in reference [4] that the hysteresis loops are identical in the thermodynamic limit
20. L. Viana, A.J. Bray, J. Phys. C. **18**, 3037 (1985)
21. V. Basso, A. Magni, private communication
22. T. Schneider, E. Pytte, Phys. Rev. B **15**, 1519 (1977)
23. S. Franz, private communication
24. Preliminary numerical simulations of the 1-d RFIM show that the typical magnetization $m(g = 0, H)$ of the metastable states is (slightly) different from the mean magnetization of the states that are obtained dynamically by starting from random initial configurations of maximal entropy (i.e. with $s_i = \pm 1$ with probability 1/2); this latter process corresponds to an instantaneous "quench" of the system from an infinite temperature to $T = 0$. This result (if confirmed) implies that the basins of attraction of the metastable states do not have the same size under the one-spin-flip dynamics.
25. R.O. Sokolovskii, M.E. Cates, T.G. Sokolovska, Phys. Rev. E **68**, 026124 (2003)
26. V. Basso, A. Magni, Physica B **343**, 275 (2004)
27. Note that the reverse (inner) trajectories which bound the two domains of existence of the H-states start from the last available states on the convex parts of the major loop (spinodals) and meet the concave, inaccessible parts of that loop at the two singular points with an infinite slope. The fields at the starting and meeting points are separated by $2J$, which shows that the proof given by P. Shukla in Phys. Rev. E **63**, 27102 (2001) is applicable even in the case of a discontinuous hysteresis loop